Stimuli responsive upconversion luminescence nanomaterials and films for various applications

Ming-Kiu Tsang, Gongxun Bai and Jianhua Hao*

Upconversion luminescence (UCL) refers to nonlinear optical processes, which can convert near-infrared photons to short-wavelength emission. Recent advances in nanotechnology have contributed to the development of photon upconversion materials as promising new generation candidates of fluorescent bioprobes and spectral converters for biomedical and optoelectronic applications. Apart from the remarkable photoluminescence of the materials under photon excitation, some UCL materials may exhibit intrinsic magnetic, ferroelectric, X-ray absorption properties, and so on. These interesting characteristics provide an opportunity for us to couple a single stimulus or multiple stimuli (electric field, magnetic field, X-ray, electron beam, temperature and pH, etc.) to various types of UCL materials. In this review, we will primarily focus on the stimuli responsive properties of UCL materials beyond light–matter interaction, which can aid both fundamental research and widespread applications of the materials. The mechanisms of the response to various stimuli in the UCL materials are discussed. This article will also highlight recent advances in the development of these materials in response to various stimuli and their applications in multimodal bioimaging, drug delivery and release, electro-optical devices, magnetic, temperature and pH sensors and multiple anti-counterfeiting inks. Lastly, we will present potential directions of future research and challenging issues which arise in expanding the applications of stimuli responsive UCL materials.

1. Introduction

Stimuli responsive materials can be defined as the materials that respond to light, magnetic or electric field, temperature, ionic strength, pH, and so on.[1–3] Nowadays, numerous studies on stimuli responses have focused on polymers, which are named as ''smart'' and stimuli responsive polymers.[4]

Smart polymers are playing important roles in a wide range of applications, including magnetic field guided drug delivery,[5] shape memory composites[6] and self-healing application,[7] to name a few. Comparatively, the fundamental issues of stimuli responses in upconversion luminescence (UCL) materials are rarely addressed and summarized as a specific subject, although many researchers have demonstrated a variety of promising applications based on the stimulus response of UCL materials. It is known that the UCL process is a nonlinear optical process which involves sequential absorption of two or more lower excitation photons and results in emission of higher energy photons.[8] Recently, UCL materials have drawn considerable attention and have been applied in diverse fields such as bioimaging, bio-sensing, optoelectronic devices and therapies,[9–13] owing to the striking energy transformation. Trivalent lanthanide ion (Ln^{3+}) doped UCL materials can response to near-infrared (NIR) excitation, e.g. 980 nm diode laser, and therefore emit UCL emission, displaying superior features, such as narrow and sharp 4f–4f transitions, long-lived luminescence, high penetration depth and large anti-stoke shift emission. In particular, the property of deep penetration favors the promising application of UCL materials in biological tissues. To date, UCL has been mainly classified into four types, namely excited state absorption (ESA), energy transfer upconversion (ETU), photon avalanche (PA) and energy migration upconversion (EMU).[9,14,15] ESA can be realized by UCL host materials that are singly doped with activator ions, such as Er^{3+} ions[16–28] while ETU enhances UC efficiency by co-doping a pair of sensitizer-activator ions into the host matrix, e.g. Yb/Er, Yb/Ho and Yb/Tm,[29–50] because Yb^{3+} ions demonstrate a high absorption cross-section in the NIR region (B980 nm) and well matching with the energy level of Ln activator ions. Therefore, UCL emission of two, three, four even five[51] photons can be realized by different combinations of dopants. Very recently, Liu's group demonstrated the EMU process in a core–shell $NaGdF_4@NaGdF_4$ system,[15] where energy can be migrated from the core to the sublattice to tune UCL through the core–shell structure.

Apart from the remarkable photoluminescence (PL), it should be emphasized that this class of UCL material can provide extra physical properties. For example, Gd^{3+} ions are known to possess paramagnetic properties under magnetic field. There are some types of UCL host composed of Gd^{3+} ions, such as $NaGdF_4$,[48,52–57] $BaGdF_5$,[58–61] GdF_3[62–64] and $KGdF_4$.[47,65–67] Besides magnetism, some ferroelectric materials, such as $BaTiO_3$ (BTO),[22,68–70] and $Bi_4Ti_3O_{12}$,[71] doped with Ln^{3+} ions may present both ferroelectric and UCL properties. Note that Ln^{3+} ions belong to heavy elements, which show high X-ray attenuation coefficients (XACs) and K-edge energies.[72] In principle, the XACs and K-edge energies increase across the Ln series in the periodic table. Fig. 1 summarizes the stimuli response of UCL materials towards magnetic and electric fields, high energy sources, temperature and pH. The nonlinear UCL process is either affected or unaffected by the various external stimuli. In fact, these external triggers definitely manifest the multifunctional nature of UCL materials and expand applications in whatever case.

Recent advances in nanotechnology have contributed to the development of photon upconversion nanocrystals (UCNCs) in numerous applications, including multimodal bioimaging, biodetection, drug delivery, phototherapy, photocatalysis, and spectral converters, which have been extensively reported and critically reviewed.[9–11,14,73–88] Previous reviews on UCL mainly
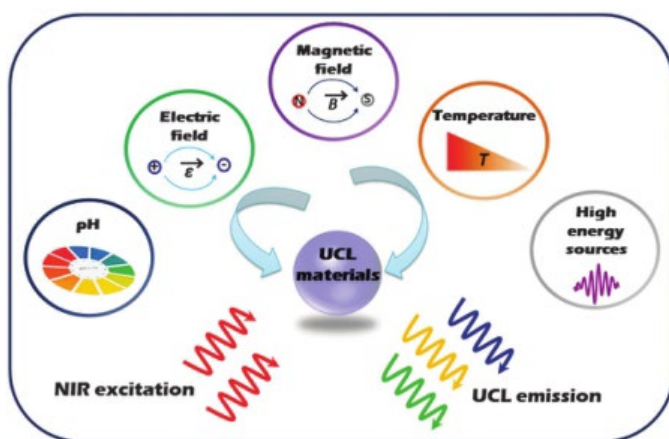

Fig. 1 Schematic illustration of summarized stimuli responses of UCL materials.

focused on the controlled synthesis, UCL tuning,[89] surface modifications and in-depth discussion of several biological fields, including in vitro and in vivo bioimaging, biodetection and therapeutic applications. So far, there have been no review to provide a unified picture of stimuli responsive properties of UCL materials and broad overview of various applications. Therefore, this review article will primarily focus on the stimuli responses of UCL materials and multifunctional applications derived from the features of the stimuli responses. We will highlight physical mechanisms, synthesis, characterization and technological applications of stimuli-stimulated UCL materials. With this end in view, we have organized the present review as follows. In Section 2, we will describe the fundamentals and mechanisms related to the interaction between various stimuli and UCL materials with the aid of typical examples. Followed by this section, Section 3 will present the considerations of material design and synthesis for achieving the stimuli responses in UCL materials, while Section 4 will outline measurements of the UCL materials responding to various stimuli. Lastly, we will highlight the recent advances and technological applications based on the stimuli responses of UCL materials.

2. Principles of stimulus response in UCL materials

2.1 Interaction of the magnetic field with UCL materials

Some effects linking the magnetic field with light are well written in the textbook.[90] For example, in the known magneto-optic effects, the Faraday effect describes changes in light transmitted through a magnetic material, while the Kerr effect describes changes in light reflected from a magnetic surface. Since then, other related effects, such as Zeeman, Voigt and Cotton–Mouton effects, are confirmed to be due to the magnetic ordering of a material either induced by an external field or present spontaneously.[91] The so-called magneto-luminescence refers to the observed phenomena of variation in PL or electro-luminescence (EL) under externally applied magnetic field, which has been investigated in transition metal doped phosphors, two-dimensional electron gas, organic compounds, and so on, typically under the conditions of high magnetic field and low temperature. For instance, Ko¨che et al. observed magneto-luminescence in electron gas under a magnetic field of 15 T and a temperature of 290 mK in a He cryostat. Dewitz et al. recorded the magneto-luminescence of InP/GaP quantum dots in the measurements of magnetic fields of up to 60 T and temperatures of below 100 K.[92–96]

As aforementioned, the existence of magnetization is frequently observed in those UCL materials composed of magnetic elements such as Gd when magnetic field is applied. Such a type of magnetic response is ascribed to the non-interacting localized nature of the magnetic moment in the compound.[49] The ability of magnetization and relaxation of the UCL materials containing magnetic elements has led to some promising applications, including bio-separation and magnetic resonance
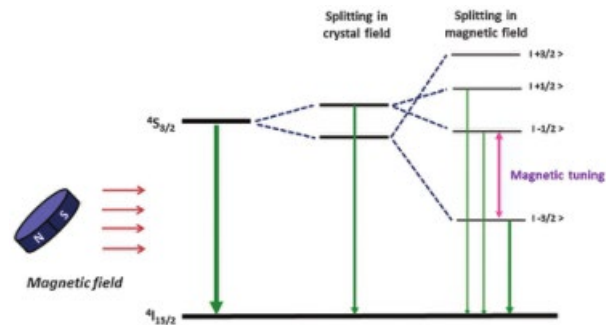

Fig. 2 A simplified energy level diagram showing the splitting of energy level $4S_{3/2}$ of the Er3+ ion in which the gap between the Zeeman levels $|\text{À}1/2\rangle$ and $|\text{À}3/2\rangle$ increases with external magnetic field.

imaging (MRI) which will be described in later section. In contrast, only limited reports have observed magneto-luminescence in UCL materials so far.[97–99] The related mechanism of the magneto-luminescence effect in UCL materials was explained by the Zeeman splitting of the energy level in Ln activator ions (e.g., Er3+ ions). Fig. 2 shows a simplified energy level diagram of Er3+ ions with $4S_{3/2}$ and $4I_{15/2}$ states only. Owing to the crystal field of the UCL material under external magnetic field, the $4S_{3/2}$ state of Er3+ ions splits into four degenerate states by the Zeeman effect, namely $|+3/2\rangle$, $|\text{À}3/2\rangle$, $|+1/2\rangle$, $|\text{À}1/2\rangle$. The separation between $|\text{À}3/2\rangle$ and $|\text{À}1/2\rangle$ increases with increasing magnetic field. This leads to a larger splitting of the $|\text{Æ}3/2\rangle$ doublet and a negligible radiative probability from $|+3/2\rangle$ to $|\text{À}3/2\rangle$. At the same time, most of the UCL emissions come from the lowest $|\text{À}3/2\rangle$ level in the $4S_{3/2}$ quartet. Therefore, the external magnetic field decreases the visible UCL emission intensity from the $4S_{3/2}$ quartet of Er3+ ions.[97]

2.2 Interaction of the electric field with UCL materials

It is known that the optical property of UCL materials is affected by the uneven components contributed by the crystal field around Ln activator ions in low symmetry hosts. This principle can be used to explain the UCL enhancement in the hexagonal phase of most common $NaYF_4$ relative to its cubic counterpart.[100] Conventionally, variations in host symmetry and the crystal field of UCL materials are routinely achieved by chemical approaches, i.e. changing the composition and the phase of the host. In comparison, the electric field responsive action of UCL materials is a physical method that modulates the lattice site symmetry around the activator ions in the same host in in situ and real-time manners. The resultant symmetry changes contribute to different transition probability that leads to UCL modification (Fig. 3).

According to classical Judd–Ofelt (J–O) theory,[101,102] the spontaneous emission probability A_{ed} for an electric dipole (ED) transition between initial J manifold $|[S, L] J\rangle$ and a final J manifold $|[S_0, L_0] J_0\rangle$ is given by eqn (1),

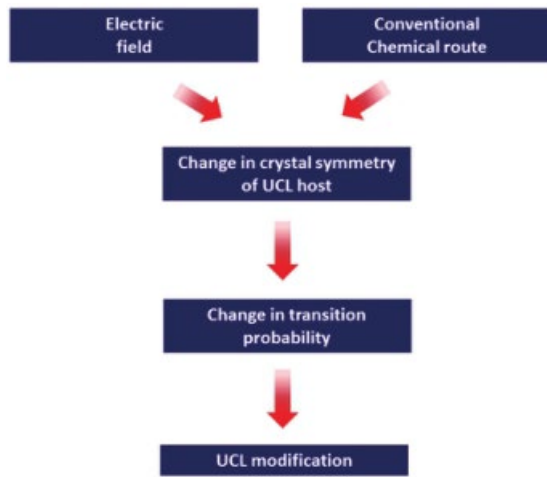$$A_{ed} = \frac{64\pi^4 e^2}{3h(2J+1)\lambda^3} \frac{n(n^2+2)^2}{9} S_{ed} \qquad (1)$$

Fig. 3 A flowchart to elucidate the electric field responsive and conventional chemical route towards the UCL emission change.

Fig. 4 The tetragonal lattice of Er-doped BTO thin films (a) without and (b) with an external electric field E. (Adapted from ref. 68. Copyright 2013. Wiley-VCH Verlag GmbH & Co. KGaA, Weinheim. Reproduced with permission.)

where e is the electron charge, l is the mean wavelength of the transition, n is the refractive index at the wavelength of the transition and h is the Planck constant. The ED line strength S_{ed} is given by eqn (2),

$$S_{ed} = \sum_{t=2,4,6} \Omega_t |\langle 4f^n \psi; L \| J k U_{(t)} k 4f^n \psi'; L' \| J' \rangle|^2 \tag{2}$$

where three terms $\langle J U_{(t)} J \rangle$ are reduced matrix elements of the unit tensor operators, and three J–O intensity parameters Ω_t (t = 2, 4, 6) contain the effect of the crystal-field terms, radial integrals of an electron, and so on. Among the complicated elements, the Ω_2 term dominates a so-called hypersensitive transition and this parameter is known to be closely associated with asymmetry of the lanthanide ion sites. The lower symmetry usually contributes to the larger Ω_2.

In order to observe the electric effect on the UCL spectra, it is crucial to design a combination of the Ln ion activator and the suitable host, which should facilitate the variation of asymmetry of activator ion sites by adjusting the electric field. Herein, BTO:Yb/Er (Fig. 4) is used as a typical combination example to further elaborate the electric field response of UCL materials. BTO is selected as the ferroelectric UCL host because it has been regarded as a model system for investigating crystal structure transformation under mechanical stress, electric field, and temperature. The Er^{3+} ion as a Ln activator ion is composed of an incompletely filled 4f inner shell and two closed outer shells. The BTO lattice is non-centrosymmetric in the tetragonal phase with the point group 4mm (C_{4v}) at room temperature, and Ti is shifted related to the negatively charged oxygen atoms (Fig. 4(a)), producing polarization. A previous study has indicated that the doping Er^{3+} ions can substitute Ti^{4+} ions in BTO,[22] hence Er^{3+} ions in the lattice are non-centrosymmetric even there is no electric field.

When electric field is applied on the combined system, the BTO lattice will be distorted and result in lower crystal symmetry around Er^{3+} ions (Fig. 4(b)). In principle, the lower symmetry at 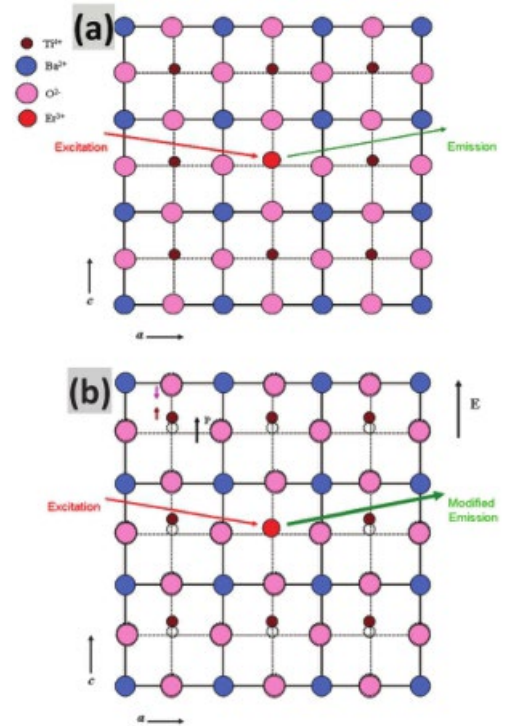the site of Ln ions means that the more uneven crystal-field components can mix opposite parity into 4f configurational levels and subsequently increase the electric dipole transition probabilities of the dopant ions. Consequently, the hypersensitiveness of the transitions of Er^{3+} ions results in the electric field response of BTO.

2.3 Interaction of high-energy sources with UCL materials

UCL materials are found to be responsive to high energy sources, such as X-ray and electron beams. The X-ray response of UCL materials arises as a result of the X-ray attenuating nature of the doped Ln elements. When materials are irradiated by X-ray, X-ray will either penetrate or be absorbed or scattered by the material. The latter two phenomena contribute to the decrease of X-ray and referred to as X-ray attenuation. The attenuation amount can be quantified by eqn (3) as follows,

$$I = I_0 e^{-\mu x} \tag{3}$$

where I and I_0 are the transmitted X-ray intensity and original intensity, respectively. m is the XAC and x is the penetrating depth of X-ray.

When X-ray interacts with materials, there are mainly three types of processes, namely coherent scattering, Compton scattering and the photoelectric effect. Briefly, coherent scattering means the emission of same energy photons by the material when the material absorbs X-ray. Compton scattering is the collision of X-ray photons with outer shell electrons of the target material and part of the X-ray energy is transferred to the material,

Table 1 X-ray mass attenuation coefficient of elements, including the ones in the Ln series, common UC host elements and traditional elements for X-ray absorption at 100 keV (cm$_2$ g^{-1})[103]

Element	Atomic number	K-edge energy (keV)	X-ray mass attenuation coefficient at 100 keV (cm$_2$ g^{-1})
Y	39	17.0	0.90
I	53	33.2	1.94
Ba	56	37.4	2.20
La	57	38.9	2.31
Ce	58	40.4	2.45
Pr	59	42.0	2.59
Nd	60	43.6	2.69
Pm	61	45.2	2.84
Sm	62	46.8	2.90
Eu	63	48.5	3.04
Gd	64	50.2	3.11
Tb	65	52.0	3.25
Dy	66	53.8	3.36
Ho	67	55.6	3.49
Er	68	57.5	3.63
Tm	69	59.4	3.78
Yb	70	61.3	3.88
Lu	71	63.3	4.03
Au	79	80.7	5.16

Fig. 5 XACs of commonly doped Ln elements in UCL materials and conventional elements for X-ray imaging over the 30–100 keV energy range.[103]

and then the X-ray photons will be deflected. Lastly, the photo-electric effect is due to the collision between X-ray photons and the inner shell electrons (e.g., K and L shell), and then the material emits characteristic X-ray photons in random directions. Moreover, the incoming X-ray photons should possess energy greater than the binding energy (K-edge energy) of the material to facilitate the photoelectric effect. In fact, Compton scattering and the photoelectric effect are prominent in clinical X-ray imaging applications.[72] Table 1 shows the XACs and K-edge energies of the whole Ln series and some common metallic elements for X-ray imaging. It should be noted that the Ln elements exhibit increasing XACs and K-edge energies as the atomic number increases, therefore Ln elements have the ability to produce enhanced contrast in water or small animals. Such striking X-ray-stimulated features enable one to use UCL materials as potential contrasts in in vitro and in vivo X-ray medical imaging which will be discussed in Section 5. Interestingly, combinations of different Ln dopants in UCL materials can show different attenuation coefficients at various energy ranges. Fig. 5 shows the XACs of some common Ln elements and traditional elements (Ba and I) for X-ray imaging in the 30–100 keV energy range, in which the first data point of each curve corresponds to the K-edge energy of the element.

Although Ba and I show high XACs and low K-edge energies, the XACs of Gd, Yb and Er are higher than those of Ba and I under the same photon energy. Importantly, the differences in XACs at various energy ranges of Ln elements are beneficial for different groups of patients such as adults and children in X-ray medical imaging. Therefore, Ln doped UCL materials are attractive as X-ray medical imaging probes.

The electron beam can also interact intensively with a variety of luminescent materials because of the existence of doped Ln luminescent centres. However, it is important to distinguish the order of magnitude of excitation energy of the incident electron beam relative to that of conventional photon excitation in PL.
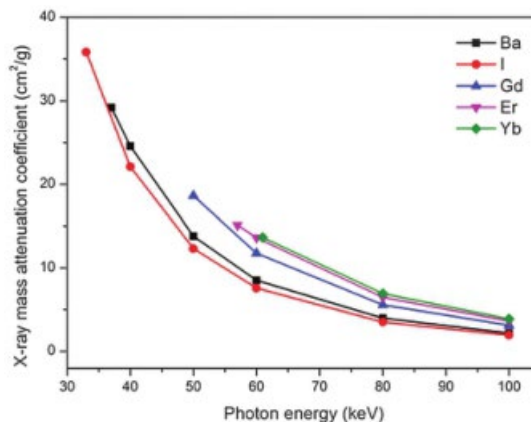
Typically, electron beams are in the magnitude of keV while photons are in eV.[104] Intense cathodoluminescence (CL) emissions were reported to be observed in down-conversion luminescent (DCL)[57,65,105–109] and UCL materials.[48,49,110] In fact, the fundamentals of CL in these materials are described by the general range-energy R expression as,

$$R = bE_n \qquad (4)$$

where b is a constant related to the material and n is a constant assumed to be independent of material. However, it was later confirmed by Feldman that n should be a constant that also depends on materials. Therefore, b and n are related by the equations as follows:

$$b = 250A/rZ_{n/2} \qquad (5)$$

$$n = 1.2/(1 - 0.29\log_{10} Z) \qquad (6)$$

By substituting b into eqn (4), one could yield the explicit form of the range expression as:

$$R = 250(A/r)(E/Z_{1/2})_n \qquad (7)$$

where r is the bulk density; A is the atomic or molecular weight of the material; Z is the atomic number or the number of electrons per molecule in the case of compounds.[111] Eqn (7) describes the penetration depth of the electron beam into the layer of luminescent materials and the depth mostly depends on the energy of the electron beam. Upon increasing energy of the electron beam, the electrons can excite more luminescent centers in the deeper region of the luminescent materials and hence resulting in more intense CL emission.

2.4 Effects of temperature and pH on UCL materials

Macroscopically, temperature is a fundamental thermal quantity in many fields of science and engineering. In a microscopic view; phonons are major factors governing the thermal conductivities. The energy of a given lattice vibration in a lattice is quantized into a quasi-particle called a phonon. Previous reports show that temperature is associated with the phonon relaxation rate
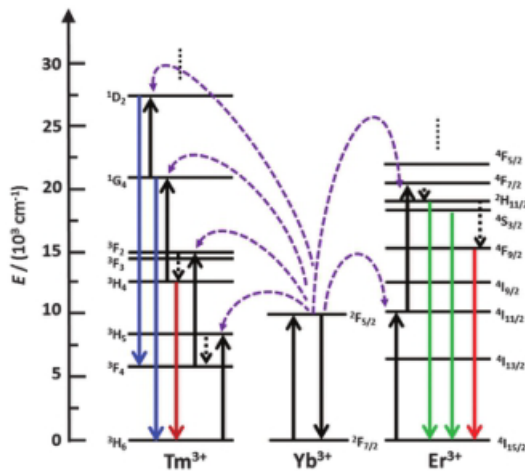
Fig. 6 Simplified energy level diagram of the Yb[3+] ion sensitized Er[3+] and Tm[3+] UCL system. The black, dashed, black dotted, and colored full arrows represent photon excitation, energy transfer, multiphonon relaxation, and emission processes, respectively.[114]

Fig. 7 Schematic illustration of the pH-induced reversible assembly of AuNPs and its effect on the switching of the UCL emission of NaYF$_4$: Yb/Er@SiO$_2$ UCNCs. (Adapted from ref. 121. Copyright 2009. Royal Society of Chemistry. Reprinted with permission.)

and hence affects the UCL property.[112,113] As a result, it is reasonable to predict that Ln doped UCL materials are sensitive to temperature because of some close energy gaps in their energy levels (e.g. Er[3+] and Tm[3+] ions). Fig. 6 shows a simplified energy level diagram of the Yb/Er or the Yb/Tm sensitizer-activator ETU pair. Er[3+] is well known for its green ($2H_{11/2}/4S_{3/2}$ - $4I_{15/2}$) and red ($4F_{9/2}$ - $4I_{15/2}$) bands while Tm[3+] for blue ($1D_2$ - $3F_4$, $1G_4$ - $3H_6$) and NIR ($3H_4$ - $3H_6$) UCL emissions.

It is important to note that there are some close energy levels in Er[3+] and Tm[3+], such as $2H_{11/2}/4S_{3/2}$ and $3F_{2,3}/3H_4$. These energy levels are separated by a few hundred wavenumbers.[115,116] Therefore, these states are highly sensitive to thermal agitation, which may serve for temperature sensing application. Taking the Er[3+] ion as an example, the temperature of the measuring system can be found using the Boltzmann law[117,118] as follows:

$$\frac{I_H}{I_S} = Ce^{\frac{-\Delta E}{kT}} \qquad (8)$$

$$C = \frac{S_H \omega_H g_H}{S_S \omega_S g_S} \qquad (9)$$

where I_H and I_S are the UCL intensity of $2H_{11/2}/4S_{3/2}$ - $4I_{15/2}$ transitions, C is a constant depending on s, o, g, which correspond to the emission cross section, angular frequency and degeneracy of the $2H_{11/2}/4S_{3/2}$ - $4I_{15/2}$ transitions, respectively. DE is the energy gap between the two states and kT E 200 cm^{-1}.[20]

Meanwhile, pH is a common chemical parameter that reflects the concentration of hydrogen ions in the medium. This parameter can affect the UCL emission of Ln doped UC materials. For instance, Capobianco's group prepared oleate-ligand free NaYF$_4$:Yb/Er UCNCs by thermal decomposition followed by acid treatment. They showed that the UCL from the UCNCs can be tuned by pH. Moreover, the red emission can be enhanced at low pH.[119] The observed red enhancement was explained by the different multi-phonon relaxation from various excited states of th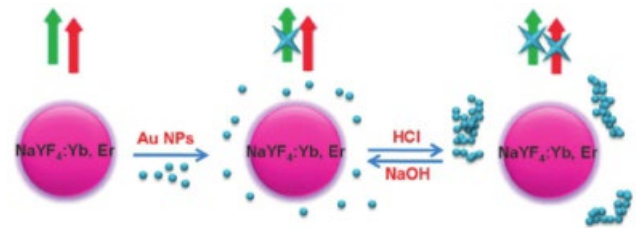e Er[3+] ions due to interactions with surface OH groups from water. Moreover, modern applications based on UCL materials are required to link or disperse UCL materials with/in other chemicals to enable many pH related applications such as targeting bioimaging, biodetection and phototherapy. Therefore, it is valuable to understand the pH responses of UCL materials in these systems. Herein, we use a core–shell NaYF$_4$:Yb/Er@SiO$_2$ and a cysteine–Au system as an example to show the working principle of the pH responsive UCL material system illustrated in Fig. 7. In such a system, Au exhibits the surface plasmonic-absorption band (SPB) which overlaps with the green UCL emission of NaYF$_4$:Yb/Er UCNCs and the cysteine linkage is pH sensitive. Upon pH changes, the linkage can be destroyed and rebuilt, leading to reversible assembly and disassembly of AuNPs. The change in morphology also caused red-shift in SPB of AuNPs. As a result, the green and red UCL emission bands are quenched at different extent and a certain pH value.[120]

3. Material design and synthesis

The issue of controlled synthesis of UCNCs has already been addressed and readers are referred to the numerous well-focused research and review articles published over the past several years.[9,14,75,83] Here, we focus on the discussion of design and synthesis of stimuli responsive UCL materials.

3.1 Material design for stimuli responses

Realization of coupling of single stimulus or multiple stimuli to the UCL material system requires state-of-the-art synthesis techniques. Accordingly, UCL materials have been prepared in a variety of forms, including nanoparticles (NPs), core–shell NPs, films and ceramics in order to meet the needs of novel applications. Table 2 shows the considerations of material design to realize the stimuli responses of UCL materials. A non-exhaustive list of typical examples capable of responding to different stimuli is given.

In general, there are several approaches to design single stimulus or multiple stimuli coupled by UCL materials. For example, (I) doping the coordinating materials into the UCL host, (II) anchoring the coordinating materials on the surface of UCL materials, and (III) growing a layer of a shell that consists of the coordinating material on the surface of UCL materials. Magnetic UCL materials can be synthesized by simply doping

Table 2 Considerations for stimuli responsive UCL material design and typical examples

Stimulus	Typical example	Ref.
Magnetic field	Gd^{3+} or Mn^{2+} ions	98
	IONPs	126
Electric field	Non-symmetric hosts	68
X-ray	Ln or Ba^{2+} ions	60
	AuNPs or shell	129
Electron beam	Er^{3+} or Tm^{3+} ions, etc.	48
Temperature	Er^{3+} or Tm^{3+} ions, etc.	211
	PNIPAM	233
pH	Amine or thiol linkage	121
	PAA or DMMA	133
	Organic dyes	138

Gd^{3+} or Mn^{2+} ions into the host because Gd^{3+} and Mn^{2+} ions have been known for their paramagnetic properties.[121] For Gd^{3+} ions, the strength of paramagnetism in UCL materials depends on the doping amount.[46] The doping of magnetic Mn^{2+} ions in UCL materials is also reported on the tunable phase and red emission in Yb/Er doped hosts, such as $NaYF_4$,[122] $NaLuF_4$ and $NaYbF_4$.[123] Besides doping, superparamagnetic iron oxide nanoparticles (IONPs), for example Fe_3O_4, can be anchored on the surface of UCL materials via cross-linkers for stronger magnetic properties compared to Gd^{3+} doped UCL materials.[124] Even so, magnetic responsive UCL materials can be designed by using the core–shell approach, which allows the formation of an inert shell without activator ions or an active shell with activator ions consisting of paramagnetic Gd^{3+} on the surface of UCL materials. Moreover, the design can be reversed by using Fe_3O_4 as the core and UCL materials as the shell.[125–127] Electric field responsive UCL materials are mostly based on the materials, whose crystal symmetry is variable upon application of electric field. As discussed in the previous section, ferroelectric host doped Ln ions such as BTO:Yb/Er are some of the good choices because of their crystal lattice being affected by electric field.

In addition to magnetic and electric fields, there are various choices of materials that allow coupling of high energy radiation to UCL materials. From Table 1, the series of Ln elements demonstrate significant XACs, and therefore common Ln doped UCL materials should possess X-ray attenuating properties. In principle, the tailoring of attenuation properties solely depends on the choice of Ln dopants. But one should keep in mind that Ln doping will also possibly affect other physical properties, such as lattice strain and UCL properties. Owing to the low phonon energy of the general formula, $ALnF_9$ where A represents the cation, the recent reported $BaYF_5$ (ref. 43) and $BaGdF_5$ (ref. 61) are confirmed to emit intense UCL via phonon mediation. Interestingly, Ba is a common element used in well-established X-ray imaging. Therefore, the Ba-based UCL host may further enhance the X-ray attenuation of UCL materials. Meanwhile, the metallic Au element is gaining popularity in the biological field because of its bio-compatibility, facile preparation and SPB properties.[128] According to Table 1, the XAC of Au is superior to Ln dopants; therefore the decoration of AuNPs or growth of Au shells on the surface of UCL materials can further enhance the attenuation ability of UCL materials. Regarding the design of electron beam responsive UCL material, the main consideration is the dopant type and concentration of UCL materials. In fact, a number of Ln activator dopants, such as Tm^{3+} and Er^{3+} ions, can effectively response to the excitation of the electron beam, leading to CL emission.[48,49,106]

Temperature sensitiveness of UCL materials is mainly due to the closeness of small energy gaps in Ln activators, such as Er^{3+} and Tm^{3+}, therefore these two types of Ln dopants are commonly used in temperature sensing applications. The UCL green and red bands of Er^{3+} ions match well with some absorption bands of organic materials, which may favor multi-sensing applications. Some polymers can be well conjugated to the UCNPs to fabricate nanocomposites for thermo-responsive applications. Thanks to the thermo-responsive property of the poly(N-isopropylacrylamide) (PNIPAM) polymer, thermo-responsive drug delivery and released systems havebeen constructed based on the PNIPAM.[129–131] Such a class of polymer has a distinct phase transition temperature called lower critical solution temperature (LCST). The LCST is tunable and the PNIPAM can collapse and become insoluble above LCST.[132] By tuning the LCST close to the body temperature of small animals, in vivo thermo-responsive applications based on UCNPs are therefore highly feasible. This promising ability has evoked the design of thermo-responsive drug delivery and release systems.

On the other hand, pH sensitive UCL materials are usually achieved indirectly via pH sensitive chemical linkages and materials. The physical properties of these linkages or materials are altered because of the change in pH, for example, one of the key issues for pH responsive drug release is the switch in polarity of surface charge in different pH environments. Surface capped polymers, such as polyacrylic acid (PAA)[133–135] and 2,3-dimethylmaleic anhydride (DMMA),[136] have been proved to exhibit a charge switching feature in various pH environments for pH responsive drug delivery and release. Also, the linkage between PEI and graphene oxide nanosheets can be intensified under increasing pH,[137] bromothymol blue (BTB) organic dye changes its absorption spectrum upon changing pH.[138] Also, the observation of reversible destruction and construction of thiol linkage in cysteine capped AuNPs under variable pH.[120]

3.2 Synthesis of stimuli responsive UCL materials

Firstly there are various synthesis techniques for preparing stimuli responsive UCNCs, including co-precipitation,[40,139–141] thermal decomposition,[32,43,45,142–144] hydrothermal,[48,58,59,66,67,145–147] sol–gel,[18,148] cation exchange,[149] flame synthesis[150,151] and combustion synthesis.[152] So far, co-precipitation, thermal decomposition and hydrothermal synthesis remain the three of the common strategies to synthesize UCNPs with high monodispersity, controllable sizes and regular shapes.[75] The co-precipitation synthesis is a low cost and simple strategy to synthesize narrow size distributed UCNCs under mild reaction conditions, although post- annealing

treatment may be needed.[13,80] van Veggel's group has synthesized single Ln-doped downconversion LaF3 nanocrystals by using ammonium di-n-octadecyldithiophosphate as a capping ligand to control the growth and enhance stabilization of the sample against aggregation.[139] Subsequently, Chow's group adopted and refined the co-precipitation method to synthesize codoped LaF3 UCNCs, the as-synthesized UCNCs exhibit very small size (B5 nm) and good dispersibility.[153] This simple technique has also been applied to synthesizing other types of UCNCs, such as NaYF4,[140,141] LuPO4 and YbPO4.[154] Hydrothermal synthesis is another approach of a low temperature reaction used for synthesizing UCNCs with controlled size and good dispersibility. The basic idea of the hydrothermal reaction is the utilization of high pressure and temperature above the critical point of the reaction mixture to increase the solubility of the reaction precursors and then the reaction rate can be speed up for the crystallization of UCNCs. Therefore, specific reaction vessels, such as Teflon-lined stainless steel autoclaves are needed to ensure and withstand high pressure for forming UCNCs. Li's group proposed a universal synthesis strategy based on the phase transfer and separation mechanism occurred at the interfaces of liquid, solid and solution (LSS).[155] Afterthat, Liu's group reported a powerful method of transforming the mixture of cubic and hexagonal phase UCNCs into the pure hexagonal phase by Gd3+ ion doping based on the hydrothermal synthesis.[156] Due to these findings, many types of UCNCs possessing different hosts, Ln doping and shapes were prepared, such as NaYF4[122,157–160] (Fig. 8(a) and (b)), NaLaF4,[161] NaGdF4[46,48,162–164] (Fig. 8(c)), NaLuF4 (Fig.8(d)),[165] BaYF5,[146] LaF3,[166–168] BaF2[169] andothers.[38,58,67,145,170–173] Hydrothermal synthesis also provides simple surface modification at the preparation stage. Hence various types of ligands can be chosen to cap on the surface of UCNCs, offering a low-cost and simple way to prepare UCNCs for biomedical applications.

Differentligands,suchas 6-aminocaproic acid,3-mercaptopropionic acid and polyethylene glycol (PEG) capped UCNPs have been synthesized by hydrothermal synthesis.[174] Recently, our group synthesized polyethylenimine (PEI) capped BaGdF5:Yb/Er and KGdF4:Yb/Er UCNPs by hydrothermal synthesis. Theas-synthesized UCNPs exhibit very small size (B10 nm) and good water dispersibility suitable for bioimaging and ultrasensitive detection of Avian influenza virus H7 subtype. Note that such hosts of UCNCs have no phase transition problem as observed in Na-based UCL materials.[59,66,175] Besides the co-precipitation and hydrothermal synthesis, thermal decomposition synthesis has proven to be successful in synthesizing highly regular and monodisperse UCNPs. Thermal decomposition developed by Yan's group involves the decomposition of La(CF3COO)3 hydrate in oleic acid (OA) and octadecene (OD) to prepare highly monodisperse LaF3 nanoplates.[176] Later on, this technique has further been applied for the synthesis of other high quality UCNCs with regular and monodisperse morphology. For example, Capobianco's group reported the thermal decomposition synthesis of NaYF4:Yb/Er(Yb/Tm) of metal trifluoroacetate in OA and OD at 315 1C, because of the presence of the capping and coordinating OA ligand, the as-prepared UCNCs present regular shape with high monodispersity.[45] Followed by this work, they refined this technique by eliminating the need for size fractionation to synthesize NaYF4 UCNCs with narrow size distribution.[177] Owing to the popularity of this technique, a series of Ln-doped UCNCs has been prepared by the thermal decomposition technique, such as NaGdF4 (Fig. 8(e–g)),[42,178–180] NaScF4,[181,182] NaLuF4,[32,183,184] BaYF5,[43] BaGdF5 (ref. 61) and KMnF3 (Fig. 8(h)).[40]

It is very common that the surface of UCNCs contains different types of functional groups, such as amino groups (NH2) and hydroxyl groups (OH), because the functional groups
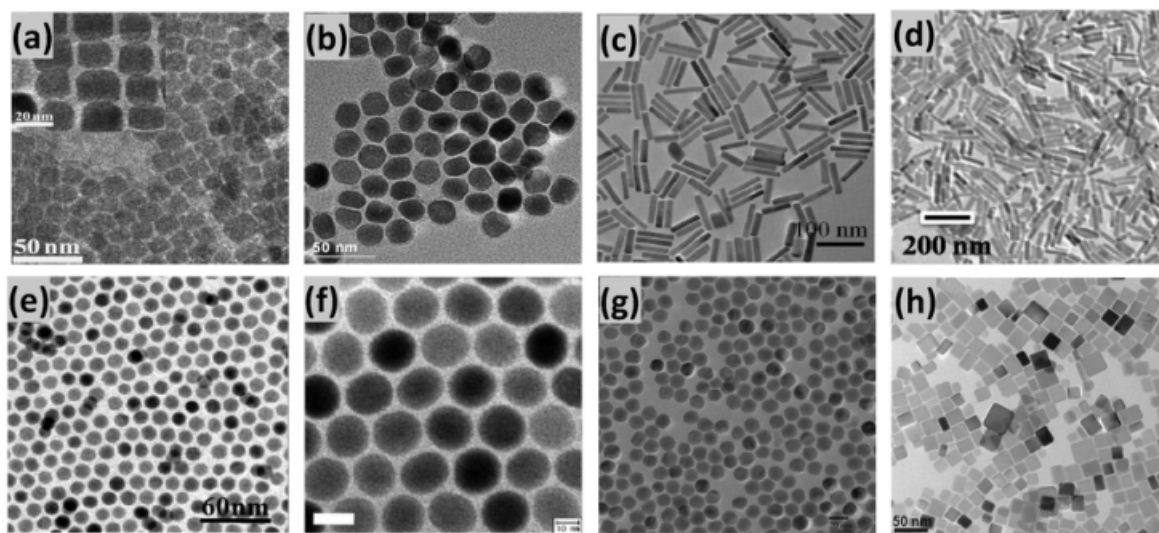

Fig. 8   TEM images of UCNCs synthesized by hydrothermal synthesis (a) NaYF4:Mn/Yb/Er (b) NaYF4:Gd/Yb/Er (c) NaGdF4:Yb/Er (d) NaLuF4:Gd/Yb/Er, thermal decomposition (e) and (f) NaGdF4:Yb/Er (g) NaGdF4:Yb/Ho and (h) KMnF3:Yb/Er. (Adapted from ref. 123, 161, 165, 166, 179, 42 and 40. Copyright 2012, 2011, 2012, 2014, 2010, 2009 and 2011. Wiley-VCH Verlag GmbH & Co. KGaA, Weinheim, Elsevier B. V., r IOP Publishing, American Chemical Society. Reproduced with permission. All rights reserved.)

can enable conjugation of UCNCs to biological systems. However, these functional groups belong to high vibrational mode groups that may quench the UCL emission from UCNCs. Moreover, the UCL emission from UCNCs is weaker than that of their bulk counterpart, and addition surface defects on NCs may form during the crystallization of UCL materials. Therefore, these factors contribute to the decrease of UC emission of UCNCs. As a result, the core–shell structure design is developed to solve this problem. In stimuli responsive UCNCs, the formation of a shell on the surface of the core can not only reduce the amount of surface defects, but also endows some features associated with stimuli responses.

To date, there have been many choices for shell materials, including inert UCL shells, active UCL shells, IO and Au shells. Numerous reports have established the formation of different undoped UC shells on the surfaceof UCNCs, such as $NaYF_4$,[185–187] and $NaGdF_4$.[188] Among them, Chow and Yi reported a remarkable enhancement of UCL emission of about 30-fold by growing a 1.5 nm thick b-$NaYF_4$ shell on the surface of the $NaYF_4$:Yb/Er(Tm) core.[186] Apart from the techniques of TEM, XRD and EDS, van Veggel's group provides evidence of core–shell $NaYF_4$@$NaGd_4$ structure by using X-ray photoelectron spectroscopy (XPS).[189] Liu's group also presented the direct evidence on surface quenching-induced luminescence modulation by epitaxial growth of a thin $NaGdF_4$ shell (B2.5 nm) on the surface of the $NaGdF_4$:Yb/Tm core of different sizes ranging from 10–25 nm. The decreased blue UC emission is stemming from the increased surface quenching sites upon decreased UCNC size. After the core–shell growth, a 450-fold enhancement was recorded in a 10 nm $NaGdF_4$:Yb/Tm core–shell UCNC, and they also found that the UC emission from core–shell UCNCs may be suppressed due to the formation of volume defects.[190] Recent reports indicate that active UCL shells are of growing interest because of their significant roles in the enhancement, tunability and increased emission modes of UCL. For example, Capobianco's group shows a design of $NaGdF_4$:Yb/Er as an active-core and $NaGdF_4$:Yb as an active-shell.[188] They observed approximately a three-fold UCL enhancement of green and red bands by the core–shell $NaGdF_4$:Yb/Er@$NaGdF_4$:Yb compared to $NaGdF_4$:Yb/Er core only UCNCs, the enhancement is attributed to the extra energy transfer from the Yb^{3+} ion in the shell to the Er^{3+} ion in the core. In a novel design, Chen's group simultaneously realized UC and DCluminescence ina core–active shell system by preparing highly monodisperse $NaGdF_4$:Yb/Tm@$NaGdF_4$:Eu core–shell multifunctional material (Fig. 9).[191] This core–shell structure is able to realize UC and DC luminescence of Eu^{3+} ions because the NIR (973 nm) excitation can penetrate through the shell to excite the Tm^{3+} ions to transfer energy to the Eu^{3+} ion in the shell while the UV excitation (273 nm) can excite the Eu^{3+} ion for conventional DC emission, respectively.

The third type of shell material is beyond UCL materials, such as Au and Fe_3O_4 shells. Importantly, the growth of these shells can couple multiple stimuli to the UCL materials, such as X-ray and the magnetic field for multifunctional applications. The growth of a gold shell should start with the attachment of Au seeds on the surface of UCL materials and the source of
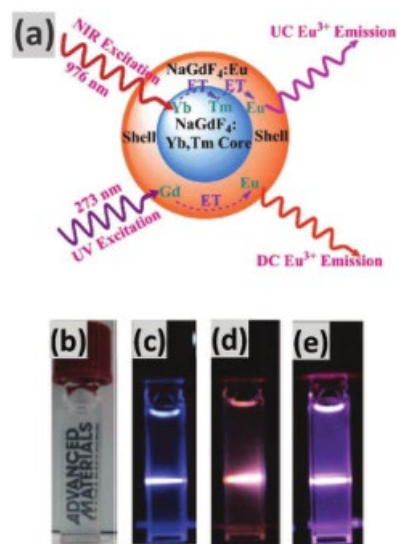

Fig. 9 (a) Schematic illustration of the general strategy to achieve the dual-mode luminescence of Eu_3+ in $NaGdF_4$ NCs. (b) A photograph shows the transparency of $NaGdF_4$:Yb,Tm–$NaGdF_4$:Eu core–shell NCs in cyclohexane solution. (c) UCL photograph of $NaGdF_4$:Yb(18 mol%), Tm(1 mol%) core only NCs in cyclohexane solution upon excitation at 976nm.(d)DCand(e)UCLphotographsof$NaGdF_4$:Yb(18mol%),Tm(1mol%)–$NaGdF_4$:Eu(10 mol%) core–shell NCs in cyclohexane solution when excited at 273 and 976 nm, respectively. (Adapted from ref. 192. Copyright 2010. Wiley-VCH Verlag GmbH & Co. KGaA, Weinheim. Reproduced with permission.)

Au seeds is typically $HAuCl_4$. However, the direct growth of Au on the UCL material surface has proven to be unsuccessful because homogeneous nucleation of Au is favored over heterogeneous nucleation of Au, and therefore the small separation between the UCL surface and Au may induce severe UCL quenching.[56] Therefore, the Au shell is usually separated by a silica[192] or an organic layer.[193] Similar to the Au shell, the growth of the Fe_3O_4 shell requires IONPs as seeds which are synthesized either prior to being added to the original UCL synthesis system,[126,127] or Fe_3O_4 precursors, which are added directly to the UCL synthesis system.[142] Besides, there are some novel core–shell designs. For example, Zhong et al. and Zeng et al. reported core–shell structures that consist of superparamagnetic Fe_3O_4@LaF_3:Yb/Er (Fig. 10(a)) and Fe_3O_4@$NaGdF_4$:Yb/Er@$NaGdF_4$@Yb/Er, respectively. Cheng et al. prepared a core–shell structure that consists of $NaYF_4$:Yb/Er@Fe_3O_4 NPs@Au (Fig. 10(b)). Benefited from the multifunctional nature grafted by the IONPs and the shell, these UCL systems are promising in magnetic targeting, bioimaging and photo therapeutic applications.[194]

UCL layer structures can be prepared by various film deposition methods. Mostly, UC materials are not grown on the substrates directly. Instead, the UC materials are deposited after synthesis and sometimes the deposition requires the assistance of medium, such as PMMA and toluene.[195] In the simplest case, UC film is prepared by dropping the colloid onto a quartz plate and dried in air.[137,196] Spin-coating is also a common technique to prepare UCL films.[197] For example, van Veggel's group synthesized $La_{0.45}Yb_{0.5}Er_{0.05}F_3$, $La_{0.75}Yb_{0.2}Tm_{0.05}F_3$, and $Yb_{0.75}La_{0.2}Eu_{0.05}F_3$
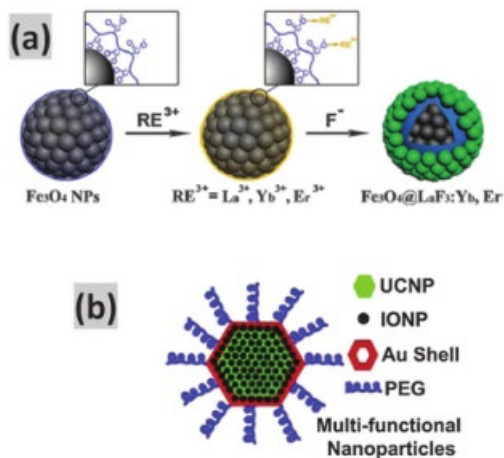
Fig. 10 (a) Schematic illustration of the process of preparing $Fe_3O_4@LaF_3$: Yb/Er core–shell material and (b) the architecture of the multi-shell structure that utilizes a $NaYF_4$:Yb/Er core, IONP as an intermediate layer and an Au shell. (Adapted from ref. 128 and 195. Copyright 2012. Royal Society of Chemistry and Elsevier B. V. Reproduced with permission.)

UCNCs by the co-precipitation method and then spin-coated the UCNCs in the form of sol–gel on a quartz plate for the generation of white light,[198] while Prasad's group spin-coated photo-patternable t-butoxycarbonyl capped a-$NaYF_4$ UCNCs for anti-fake security applications.[199] Our group reported about the fabrication of BTO:Yb/Er thin films on conductive $SrRuO_3$ (SRO)-coated $SrTiO_3$ (STO) substrates by pulsed laser deposition (PLD). Compared to bulks, the form of thin film facilitates the application of higher electric field on the UCL sample under a low bias voltage.[68] However, the BTO:Yb/Er PLD target was firstly prepared by standard solid state reactions for typical UCL ceramics[25,26,200] prior to PLD. Oxyfluoride glass-ceramics are fabricated by melting and quenching methods, which involve melting the precursors and precipitation of UC crystals in the glass matrix. The glass-ceramic UCL materials can combine the merits of low phonon energy in fluorides and chemical stability of oxides. Many types of NCs have been embedded, for instance Ba_2LaF_7,[201,202] and $BaYF_5$.[203]

4. Characterization of stimulus response

Generally speaking, various techniques of measuring conventional PL phosphors under external perturbation can be employed for the characterization of stimuli responsive UCL materials. However, some issues should be considered on the basis of UCL characteristics, such as NIR laser excitation and quite low quantum efficiency. Besides conventional photoluminescence measurements, the characterization techniques presented as follows may be used to characterize additional material properties, such as transport behaviors under electric- or magnetic-field, cathodoluminescence, photoconductivity, and magneto-luminescence. As a result, these measuring platforms are highly beneficial for characterizing multi-functional materials.
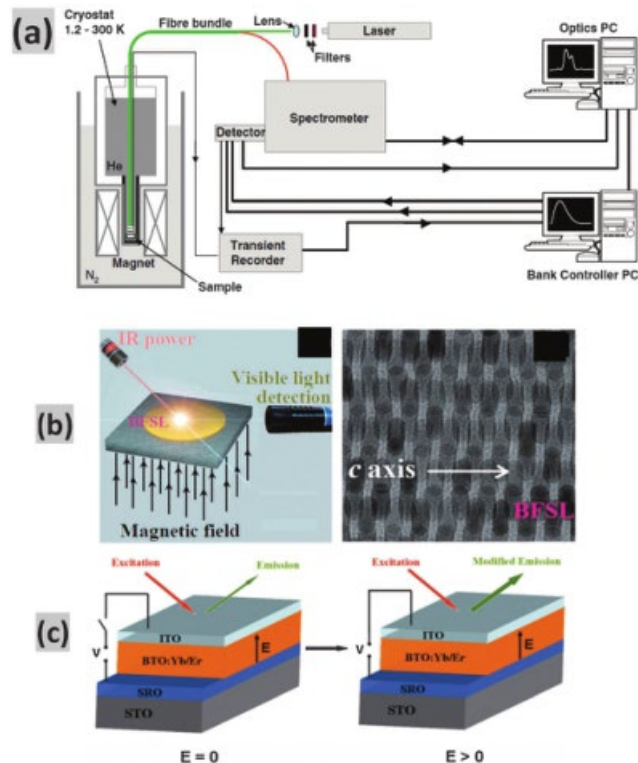

Fig. 11 (a) Measurement apparatus of luminescence under magnetic field (b) magnetic responsive measurement of UCL in $NaGdF_4$:Nd/Yb/Er BFSL. (c) The setup used to measure the UCL of a BTO:Yb/Er thin film when an external electric field is switched ''off'' (left) and ''on''(right). (Adapted from ref. 96, 98 and 68. Copyright 2012, 2013 and 2011. John and Wiley & Sons, Ltd. and Wiley-VCH Verlag GmbH & Co. KGaA, Weinheim. Reproduced with permission.)

Fig. 11(a) shows a typical setup of magneto-luminescence measurement previously used for the study of semiconductors.[95] The measurement parts comprise a dc pulsed magnet inside a cryostat and the sample is mounted between the pair of magnets. Notably, the optical components are far away from the magnet coil that can prevent risk from explosion of coils. Note that, this setup can work at the low light level. Recently, Li's group reported on the magnetic response of UCL materials.[97] The magnetic response can be measured by the scheme depicted in Fig. 11(b). The $NaGdF_4$:Nd/Yb/Er bifunctional superlattice (BFSL) film was placed on a non-magnetic substrate in a cryostat with variable temperature. The NIR excitation and the resultant UCL emission were delivered and collected by two optical fibers to the spectrometer. At the same time, a liquid-helium cooled superconductor coil was used to supply a dc magnetic field to the sample perpendicular to the film. The measurement setup of our group's work on the electric field response of BTO:Yb/Er UCL thin film is shown in Fig. 11(c), the light excitation and emission as well as the applied electric field are denoted. This is a typical parallel plate capacitor structure. The upper and lower side of the UCL material consists of conductive indium tin oxide (ITO) and SRO, respectively. Therefore, the excitation and emission light can pass through the ITO layer. Such a sandwiched structure can facilitate the manifestation of both dc and ac electric fields

across the UCL material.[68] Since this configuration is limited by the dielectric breakdown of UCL films, great attention should be paid on the insulation of the thin film during measurement to avoid potential current leakage.

The X-ray response of UCL materials can be measured in a commercial X-ray imaging machine and an X-ray computed tomography(CT)scannerextensivelyusedinclinicsandlaboratories. To quantify the X-ray attenuation, the Hounsfield (CT number, HU) unit is a parameter that determines the amount of X-ray attenuation, and this parameter is defined as,

$$CT \text{ number } = 1000 \times \frac{m_v}{m_w}$$

where m_v and m_w are the attenuation coefficient of a voxel and water, respectively.[72] Scanner parameters, such as pitch, gantry rotation time and speed, can affect the quality of scans.

Apart from single modality of X-ray imaging, it should be pointed out that a synergistic combination of various techniques in a single system, such as fluorescent microscopy/X-ray imaging, and CT/MRI, is a future trend of medical imaging technologies. Most recently, dual-modal X-ray and UC measurement have been integrated in a single system (e.g., Carestream FX PRO in vivo imaging system). In this case, simultaneous X-ray and UC bioimaging taken from small animal after the injection of the UCL nanoprobes can be tested by the multimodal bioimaging system equipped with an external 980 nm NIR laser as the excitation source and X-ray imaging accessory.[146,165] From Table 1, the attenuation coefficients of Ln elements increase with K-edge energies, implying that the combinations of different Ln elements in the host matrix can enable different ranges of CT scanning.

For the characterization of CL arising from the interaction between electron beams and phosphors, most researchers made use of conventional scanning electron microscopy (SEM) facility and performed CL spectral measurements in a high vacuum. Comparatively, we obtained CL emission using a home-made system modified from a RELIOTRON III CL luminoscope with a cold cathode electron gun. Therefore, our measurements can be performed at a higher relative pressure compared to those of other studies. Low-voltage CL and UCL spectra were measured using an Ocean Optics S4000 CCD spectrometer with a single-strand UV/VIS optical fiber. Moreover, photoconductivity and UCL emission of the samples under NIR laser irradiation can be simultaneously tested in a vacuum.[204] Loading different samples on the sample holder, which is controlled using an x–y positioner, facilitated measuring the emission of the samples in sequence under the same conditions.

Regarding pH responsive measurements, digital pH sensors and standard pH buffers are frequently used to monitor a precise pH environment for pH responsive UCL measurements. On the other hand, temperature responsive UCL measurements have some variants in designs for the control of measuring temperature. For example, a NIR laser can be employed as both excitation and heating source to heat up the UCL material. A thermocouple is in contact with the material to monitor the temperature[205,206] while some groups used furnace[23,207] or
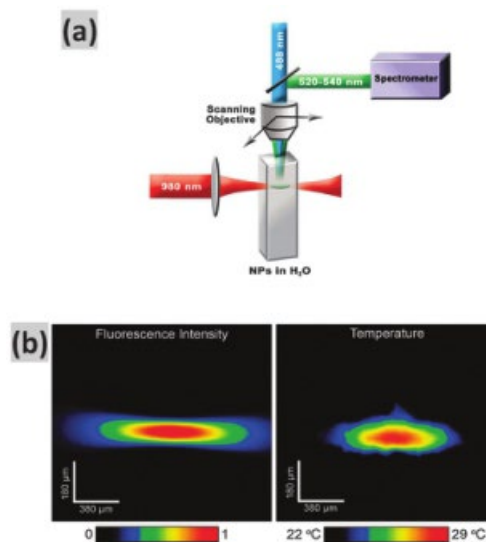

Fig. 12 (a) Schematic of the pump–probe setup used to measure the temperature profile created by heating a colloidal solution of NaYF$_4$:Yb/Er UCNCs in water with a 980 nm diode laser (pump beam) and subsequently scanned with a 488 nm argon laser (probe beam). (b) Left: confocal image of the980 nmexcited UCL (pump absorbedprofile). Right: thermal image ofthe spot created by the 980 nm pump beam. (Adapted from ref. 212. Copyright 2010. American Chemical Society. Reproduced with permission.)

cooling–heating systems to precisely measure temperatures.[208–210] Vetrone et al. built a set-up by using a pump–probe and a fiber-coupled confocal microscope connected to a high-resolution spectrometer. The magnitude and distribution of temperature of colloidal UCNCs can be measured and imaged by using the system (Fig. 12). A 980 nm diode laser and a 488 nm argon laser were used as the excitation and the probe beam, respectively. In this way, the objective can collect the luminescence generated by the samples.[211]

5. Applications of UCL materials

In recent years, the strategies based on the interaction between various stimuli and UCL materials have been demonstrated to be very attractive in multifunctional applications, ranging from biomedical to photonic areas.

5.1 Multimodal bioimaging

A variety of bioimaging techniques are routinely used in lab research and clinical applications. The bioimaging techniques based on UCL materials as probes or contrast agents include in vitro or in vivo fluorescence imaging, MRI, X-ray imaging, CT, positron emission tomography (PET) and single photon emission computed tomography (SPECT). Among them, MRI, X-ray imaging and CT are the means on the basis of the multi-stimuli response nature of UCL materials which have been discussed in this article, while PET and SPECT are achieved by incorporating radioactive tracers into UCL materials for image formation.

Table 3 lists merits and limitations of each bioimaging technique. Apparently, no single imaging technique is capable

Table 3 Comparison of merits and limitations of various bioimaging techniques and related systems

Techniques	Merits	Limitations	Imaging systems
UCL	Good planar resolution.	Limited penetration for in vivo imaging.	Confocal microscope equipped with NIR laser.
	High sensitivity.	No 3D information.	
MRI	Non-ionizing radiation.	Not suitable for patients consist of metallic parts.	Commercial 3T MRI scanners.
	Useful for imaging soft tissues.	Not able to image low hydrogen content parts.	
X-ray CT	High resolution. 3D detail of soft tissues.	Ionizing radiation. Low sensitivity.	Commercial CT scanners.
PET	Able to provide localized functions of organs.	Use of radioactive isotopes.	Gamma ray cameras.
		Costly scans.	
SPECT	Able to provide true 3D information. Cheaper scan compared to PET.	Use of radioactive isotope. Inferior accuracy in scanning deep activities in brain.	Gamma ray cameras.

of fulfilling all of the needs. Therefore, it would be desirable to develop multiple complementary imaging modalities. For most imaging modes, the contrast of imaging is potentially enhanced through the use of contrast agents. Each modality differs from another in terms of spatial and temporal resolution, anatomical and molecular details, and imaging depth. Hence the concept of complementing the strengths of one imaging modality with those of another has come to the fore and been further bolstered by the development of fused instruments. Such synergistic combinations of these bioimaging techniques can enable the strengths of each bioimaging technique to compensate the weakness of other techniques. In any synergistic bioimaging system, the utilization of a multimodal bioimaging agent is essential in order to prevent injections of more than one contrast agent into the body, which can reduce the number of possible adverse effects due to injection of multiple contrast agents. However, further development of such a new generation of biomedical imaging is currently hindered due to the lack of the ideal multimodal imaging agent. Therefore, it is interesting to investigate whether UCNCs have the potential to meet the requirements of multimodal bioimaging agents served for the attractive synergistic bioimaging techniques, e.g. UCL/MRI, UCL/X-ray CT, UCL/PET and UCL/MRI/X-ray CT or PET.

Owing to the seven unpaired 4f electrons, Gd_{3+} ions can change the spin–lattice relaxation of the protons in water to enable T_1-weighted MRI imaging. There are mainly two methods to realize UCL/MRI dual modal bioimaging: (I) doping Gd_{3+} ions into the host matrix, and (II) growing a shell on UCNCs consisting of the Gd element. For method (I), we have developed a dual modal UCL/MRI system based on amine functionalized single compound of $BaGdF_5$:Yb/Er UCNCs that exhibit a peak magnetization of 0.95 emu $gà1$ and a T_1 relaxation constant of 1.194 $mMÀ1$ $sÀ1$. With the UCNCs, both UCL cellular and MRI contrast have been demonstrated at various molar concentrations.[59] Other UCL/MRI systems based on method (I) include $NaGdF_4$:Yb/Er(Tm)[178,212,213] and $NaYF_4$:Yb/Er/Gd.[214,215] For method (II), $NaYF_4$:Yb/Er@$NaGdF_4$[216,217] and $NaYbF_4$:Tm@$NaGdF_4$[218] are used in X-ray CT or conventional X-ray imaging based on

the X-ray attenuation property of Ln dopants in UC materials. Particularly, the former technique is able to provide 3D images of internal organs achieved by computer processed X-ray to render 3D volumetric information of specific organs or tissues for diagnostic applications while the latter can only present 2D information on organs. Many Ln doped systems have been reported for UCL/X-ray CT dual modal bioimaging, such as $NaGdF_4$,[219] $NaYbF_4$,[220] and $NaYF_4$.[221] Very recently, Zeng et al. demonstrated dual-modal UCL/X-ray imaging by using ligand free $NaLuF_4$:Gd/Yb/Er nanorods. In this work, the X-ray signal matched with the UCL in the lung of a sacrificed nude mouse, indicating a successful example of synergistic bioimaging (Fig. 13(a)). Importantly, the nanorods exhibited enhanced visualization of blood vessel in X-ray and UCL bioimaging compared to that without nanorods (Fig. 13(b) and (c)). These results suggest that the UCL nanorods are some of the promising candidates for angiography imaging in disease diagnostic applications.[165]

Beyond Na-based hosts, our group has also synthesized PEG capped $BaGdF_5$:Yb/Er by one-step hydrothermal synthesis. Such a host consists of Ba and other Ln elements, possessing different K-edge energies, and therefore this host can be used as an X-ray CT agent for various groups of patients. Importantly, we have demonstrated in vivo CT images with enhanced signals of spleen of a mouse for 2 h, indicating that the UCNPs can be used as CT contrast agents for improving the detection of splenic diseases. (Fig. 13(d)).[60] Other Ba-based hosts including BaF_5[146] and $BaYbF_5$[222] are reported to demonstrate dual modal UCL/CT bioimaging applications. Interestingly, $BaYbF_5$ UCNCs can also serve as irradiation dose enhancers in tumors during radiotherapy.[222] PET belongs to a type of nuclear medical imaging technique that is capable of producing 3D images of the body by detecting the pair of g radiation emitted indirectly by a positron emitting radionuclide. To date, ^{18}F has been a well-established radionuclide for PET whole body imaging and quick coupling of ^{18}F into UCL materials for high reaction yield is very important because ^{18}F has short lifetime. Li's group provided a convenient and simple way to couple ^{18}F to $NaYF_4$ UCNCs. Moreover, they had successfully imaged the spleen and
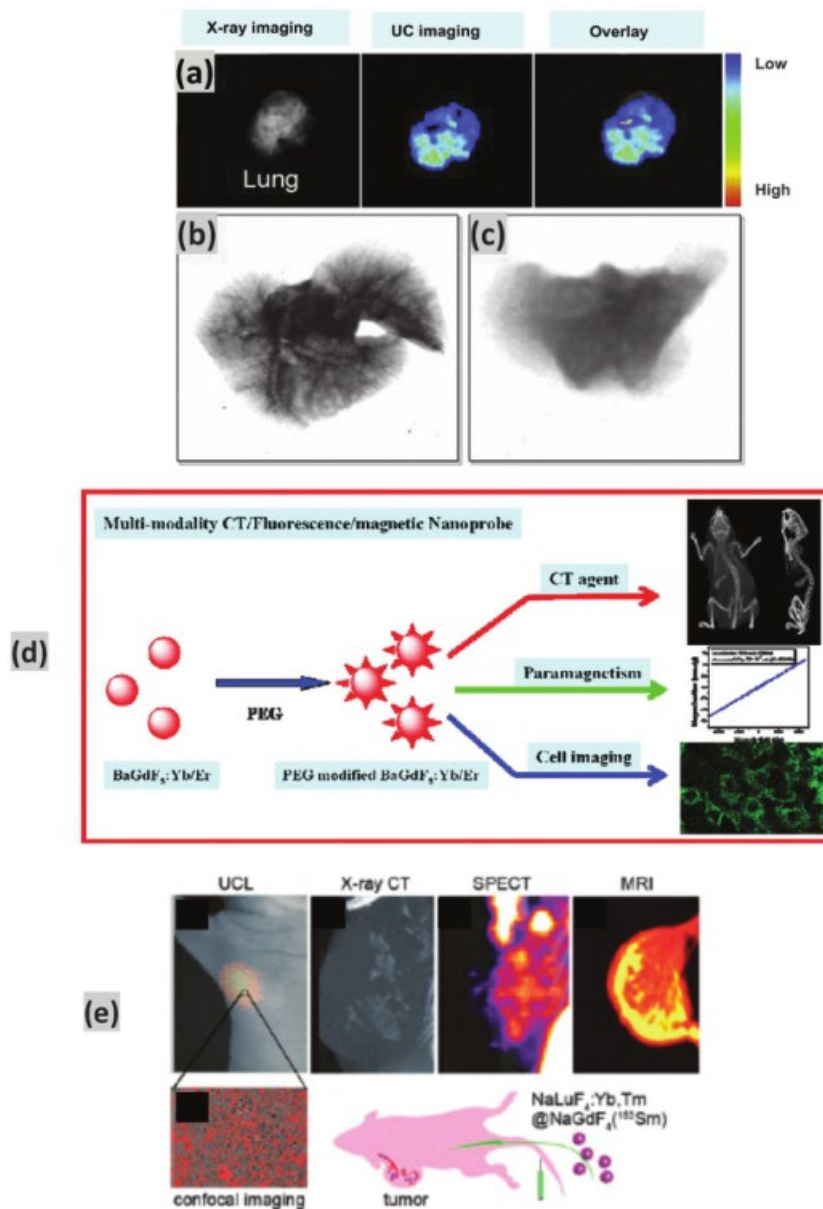
Fig. 13 (a) Dual modal X-ray/UCL bioimaging of the lung of a scarified nude mouse after 0.5 h intravenous injection of the ligand-free NaLuF$_4$:Gd/Yb/Er nanorods. (b) Corresponding high resolution X-ray imaging of the lung, demonstrating the significant visualization of the blood vessel of the lung, (c) high resolution X-ray imaging of the lung without injection of these nanoprobes, (d) trimodal UCL/MRI/X-ray CT bioimaging system based on PEG-modified BaGdF$_5$:Yb/Er UCNCs (e) four-modal (UCL/X-ray CT/SPECT/MRI) imaging of the focused tumor from a tumor-bearing nude mouse 1 h after intravenous injection of NaLuF$_4$:Yb/Tm@NaGdF$_4$(^{153}Sm). (Adapted from ref. 166, 60 and 226. Copyright 2014, 2012 and 2013. Elsevier B. V. and American Chemical Society. Reproduced with permission.)

liver of a mouse by PET through tail vein injection.[223] Li's group also addressed trimodal bioimaging, e.g. UCL/MRI/X-ray CT based on Gd complex modified NaLuF$_4$:Yb/Tm@SiO$_2$[184] and aminocaproic acid-Gd-NaYF$_4$:Yb/Er(Tm).[224] More recently, Li and co-workers reported a four modal SPECT/CT/MR/UCL bioimaging system based on a citrate group modified core–shell NaLuF$_4$:Yb,Tm@NaGdF$_4$, (^{153}Sm) probe. In addition to UCL and MRI, they observed excretion of the probe from the gall bladder to the intestine in X-ray CT.[225] Moreover, the radioactive ^{153}Sm element enables SPECT to investigate the quantitative distribution of the probe in the liver and spleen of

the mouse. The tumor angiogenesis of KB human oral tumor was also monitored simultaneously by UCL/MRI/X-ray CT/SPECT as shown in Fig. 13(e).

5.2 Drug delivery and release

In addition to multi-modal bioimaging, UCL nanomaterials with stimulus response were found to enhance the drug delivery and release ability of anti-tumor agents. Conventional drug delivery systems are hindered by the uncontrollable drug release at the initial stage of administration. Also, the drug efficacy and biodistribution are affected by some non-specific cellular and

environment during delivery.[132] Alongside this, the drug molecules might cause adverse side effects because of failure to recognize diseased or healthy cells.[226,227] Owing to the NIR excitation, the UV emission from UCNPs can effectively cleave the linker to release the photocaged molecules on the surface of UCNPs.[228–230] NIR-responsive mesoporous silica shell (m-SiO$_2$) coated UCNPs were developed for the application of controllable drug delivery.[231] The antitumor drug doxorubicin (DOX) molecules were loaded in the m-SiO$_2$ linked to the theonitrobenzyl (NB) linker. Upon NIR excitation, the NB linkers were cleaved and facilitate drug release. Moreover, the conjugations of folic acid on the surfaces of the nano-drug carriers enabled selective drug delivery.

Apart from NIR-responsive drug delivery and release, pH and thermo-responsive drug delivery and release had also been exploited in UCNP nanocomposites. Meanwhile, a novel mesoporous g-AlO(OH) capped UCNP drug delivery and release system was constructed.[232] At low pH values, the negative surface under neutral conditions switched to a positive surface to favor the conjugation of DOX to the system. When the pH value changed to 5, a cumulative release of DOX of three-fold was observed compared to that at pH = 7.4. Lin's group reported a thermo/pH dual-responsive drug controlled release system based on core–shell NaYF$_4$:Yb/Er@m-SiO$_2$ UCNPs linked to the thermo/pH responsive polymer poly[(N-isopropylacrylamide)-co-(methacrylic acid)] (P(NIPAm-co-MAA)).[233] Fig. 14(a) and (b) show the schematic structure of the drug delivery and release system. The drug-loaded particles triggered release of the encapsulated DOX at higher temperature/low pH as presented in Fig. 14(c)–(e). Each of the drug release profile at 45 1C is higher than that at 25 1C and the whole profile is promoted at pH = 2.0. These results indicate the successful construction of the thermo/pH dual-responsive drug delivery and release system. Moreover, Fig. 14(f) presents an increased UCL emission when increasing DOX release because of decreased DOX quenched UCL emission upon releasing. Importantly, this work shows that the unique properties of the hybrid nanocarriers may provide an opportunity for developing a new generation of drug carrier which possesses a decision making process for the smart site, time and dose-selected drug release and cell imaging.

5.3 Electro-optical modulator

Our group has investigated the coupling between the electric field and UCL. As shown in Fig. 15(a),[68] the UCL can be obviously enhanced when increasing the dc bias voltage. It is observed that an enhancement factor of the main green band can reach up to 2.7. On the other hand, the red emission centered at 656 nm corresponding to $4F_{9/2}$ - $4I_{15/2}$ transition almost remains unchanged with an increase of voltage. It indicates that the emission enhancement is highly wavelength-dependent. As the enhancement factors located in the green band are much higher than those in the red band (Fig. 15(b)), the PL intensity ratio of green to red emission is significantly enhanced with increasing dc bias voltage up to 10 V, which is equivalent to an electric field of 125 kV cm^{À1} on the UCL film. To understand the difference in the enhancement factors of green and red
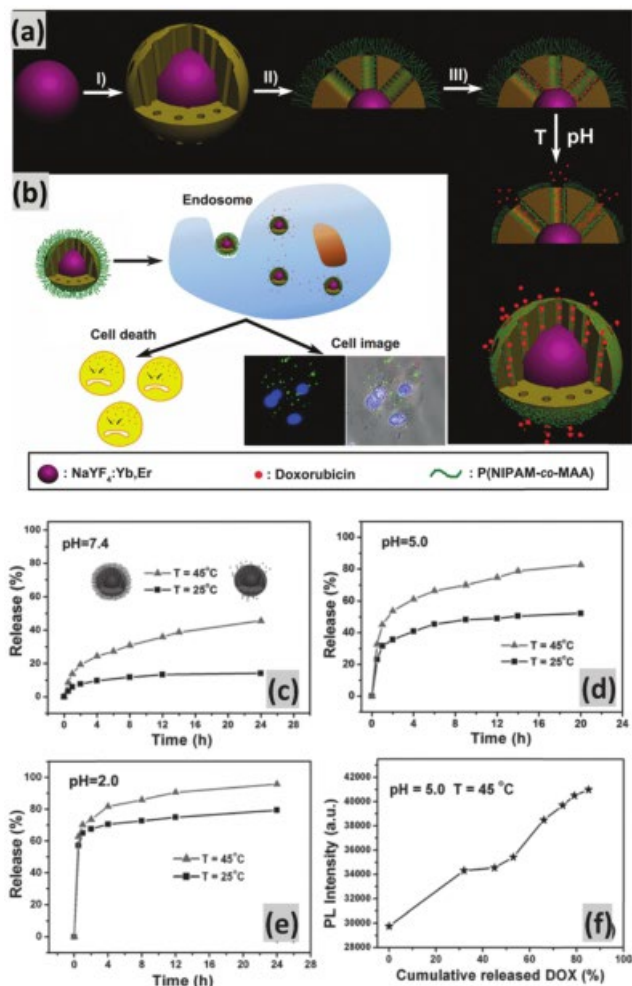

Fig. 14 (a) Synthetic route towards UCNPs@m-SiO$_2$-P(NIPAm-co-MAA): (I) cetyltrimethylammonium bromide, tetraethyl orthosilicate; (II) methacryloxypropyltrimethoxysilane, N -iso-propylacrylamide, methacrylic acid; (III) guest (DOX) loading; (IV) increase the temperature and decrease the pH value. (b) Schematic depiction of the dual function of UCNPs@m-SiO$_2$-P(NIPAm-co-MAA). Release profiles of DOX-UCNPs@m-SiO$_2$-P(NIPAm-co-MAA) in responseto temperaturechanges in PBS: (c) pH = 7.4; (d) pH = 5.0 and (e) pH = 2.0 (f) UCL intensity of UCNPs@m-SiO$_2$-P(NIPAm-co-MAA) as a function of the cumulatively released DOX. (Adapted from ref. 234. Copyright 2013. Wiley-VCH Verlag GmbH& Co. KGaA, Weinheim. Reproduced with permission.)

emission bands shown in Fig. 15(b), one should consider that the extent of the local symmetry influence on the different emission bands may vary greatly, depending on the corresponding intra-4f transitions. More importantly, the switchable symmetry in ferroelectrics provides us to realize reversible and dynamic tuning of PL emission by external electric field. As shown in Fig. 15(c), an interesting observation is that the PL intensity of the BTO:Yb/Er film under a sinusoidal ac bias can be modulated with the same frequency as that of the sinusoidal ac electric voltage. On the other hand, UCL enhancement can also be achieved by using the surface plasmonic resonance effect. Such an enhancement was due to the localized electromagnetic field effect on the surface of UCNPs. For instance, Schietinger et al. achieved plasmon-enhanced UCL
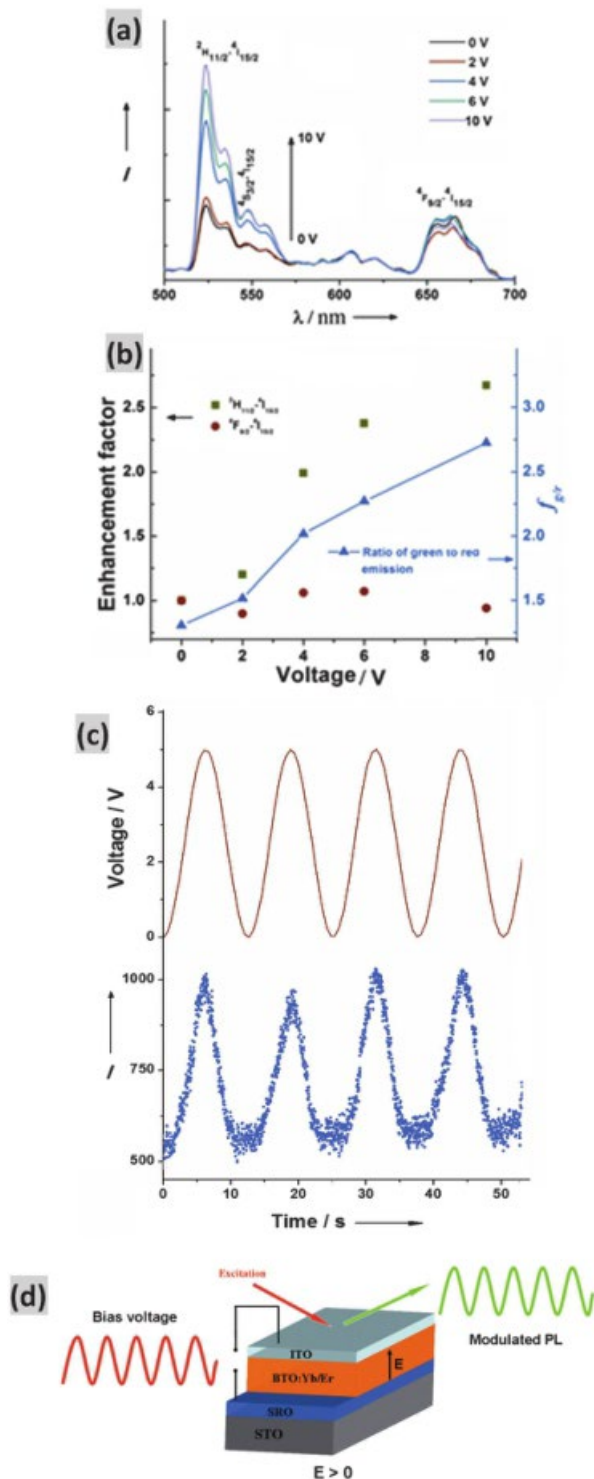
Fig. 15 (a) The UC emission spectra of the BTO:Yb/Er film under dc bias voltage ranging from 0 to 10 V. (b) The enhancement factors (left axis) for green and red UCL bands as a function of the applied dc voltage. The PL intensity ratio of green to red UCL (right axis) as a function of the applied bias voltages is also shown. The thin film sample is excited by a 980 nm diode laser. (c) Sinusoidal ac electric voltage applied to the BTO:Yb/Er film (upper in red color), and UCL emission at the wavelength of 523 nm (bottom in blue color) as a function of time while the sinusoidal ac electric field was applied on the BTO:Yb/Er film. (d) Schematic diagram of the electro-UCL modulator based on BTO:Yb/Er film. (Adapted from ref. 68. Copyright 2013. Wiley-VCH Verlag GmbH & Co. KGaA, Weinheim. Reproduced with permission.)

in NaYF$_4$:Yb/Er UCNPs.[234] By coupling Au spheres of 30 and 60 nm, they recorded an overall enhancement of 3.8 fold. In the same host material, Zhang et al. enhanced the UCL emission of NaYF$_4$:Yb/Er UCNPs by more than 2.5 by attaching AuNPs on the surface of UCNPs.[193] As a result, it should be emphasized that the modulation of UCPL cannot be achieved by conventional chemical and plasmonic methods. These results will aid further investigations of luminescence and widespread applications of UC materials because they provide an additional degree of freedom in the design of luminescent materials and devices. In these concept devices, specific emission can not only be amplified, but also be modulated electrically as shown in Fig. 15(d).

5.4 Magnetic sensors

The magnetic responsive effect in the Ln activator doped UCL materials was demonstrated by precipitating PbF$_2$:Er UCNCs in bulk oxyfluoride nano-glass ceramics.[98] The effect resulted in two orders of magnitude drop in green UCL emission ($4S_{3/2}$ - $4I_{15/2}$) under a magnetic field of up to 50 T and the drop of UCL was greatest in the range of 0–5 T. This observation has the potential for non-invasive and remote magnetic sensing. Moreover, the nanoscale magnetic sensor was suggested to achieve a sensing accuracy of 0.01 T in the range of 0 to 5 T. Despite the effort, the magnetic responsive effect observed in PbF$_2$:Er UCNCs is not pronounced as no magnetic dopant is included in the UCL material. Additional attempt was made by Rai and co-workers to observe the magnetic responsive effect of UCL emission in Gd$_2$O$_3$ UCNCs. The authors have produced a nanoscale platform with magnetic Gd^{3+} ions for the improved magnetic responsive effect, resulting in an eight fold decrease of UCL emission under varying magnetic field. The observation of the magneto-luminescence was explained in light of the Yb/Er ion cluster pair. According to the demagnetization study of the UCL material, they also found that magnetization can be retained in the UCL material for 1 h. The observed magnetic induced bistability manifests the magnetic sensing ability of the UCNCs.[99]

Until recently, Li's group has found a pronounced magnetic responsive effect in 3 mol% Nd^{3+} ion doped NaGdF$_4$:Nd/Yb/Er BFSL nanoplates at 300 and 10 K (Fig. 16(a) and (b)). UCL intensity was decreased by about 60 and 15% compared to the original value of UCL at room temperature and low temperature, respectively. In addition, the tunable magnetic responsive effect was achieved by varying the doping amount of Nd^{3+} ions, and the optimal doping concentration of Nd^{3+} ions is 4 mol% for the best magnetic responsive effect at 20 mol% Yb and 2 mol% Er (Fig. 16(c) and (d)). Their cyclic magnetic field test (Fig. 16(e)) also indicates the existence of the reversible magnetic responsive effect in the BFSL sample with less than 5% loss at 300 K and 10 K.[97] Notably, this work provides detailed explanations on the observation in Ln doped UCL materials, which may serve as a fundamental for further novel designs in future UCL magnetic sensors.

5.5 Temperature and pH sensors

UCL materials are not restricted to biosensing but also temperature and pH sensing. As discussed in the previous section,
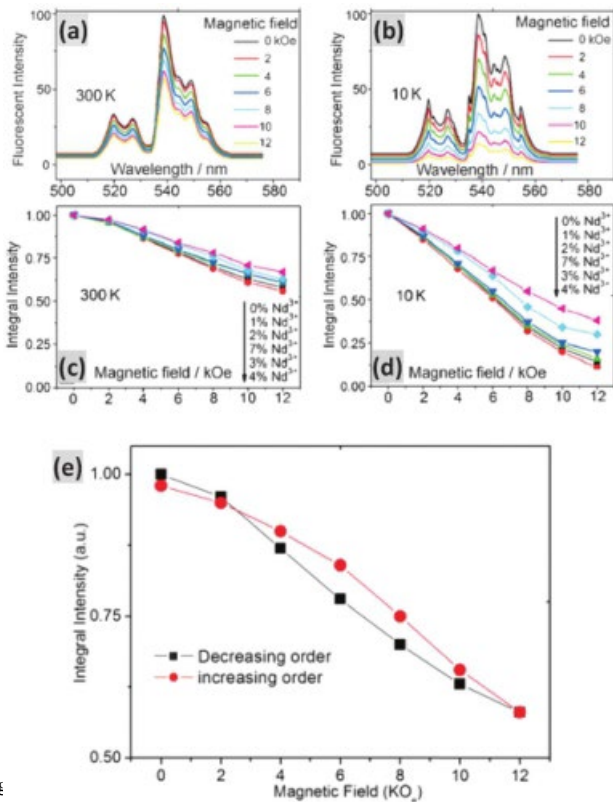
Fig[...] [...]r3+ ions in NaGdF4:Nd/Yb/Er BFSL at (a) 300 K and (b) 10 K. Dependence of the integral emission intensity of NaGdF4:Nd/Yb/Er population of Er3+ BFSL with various levels of Nd3+ doping on the applied magnetic field at (c) 300 K and (d) 10 K. (e) Appearance of hysteresis in the integral intensity of green emission from $4S_{3/2}/2H_{11/2}$ - $4I_{15/2}$ transition of Er3+ when the magnetic field is cycled in between 0 and 12 kOe. (Adapted from ref. 98. Copyright 2013. Wiley-VCH Verlag GmbH& Co. KGaA, Weinheim. Reproduced with permission.)

temperature and pH are two important quantities in the environment and organisms that require fast and sensitive sensing, and the sensitive response of Ln-doped UC materials towards temperature is rooted from the close energy levels in the activator ions. Therefore, the UCL emission intensity ratio of two close energy levels can be monitored according to the Boltzmann law. Hexagonal phase NaYF4:Yb/Er is a good candidate for thermal sensing from 298 K to 318 K because of its high emission intensity and good temperature resolution (B0.45 K), yet the resolution for Ho3+ and Tm3+ is inferior to that of Er3+ ions.117 Thanks to the deep penetration characteristics of UCL materials, Capobianco's group reported an interesting finding on monitoring the temperature in a single cell by using NaYF4:Yb/Er UCNCs as a nanothermometer. In their work, the temperature was regulated by the voltage induced thermal effect across a resistor from 298 K to 318 K and the HeLa cells exhibited morphological changes until their death (Fig. 17(a)). Moreover, the temperature sensitivity was found by observing the UCL emission intensity ratio at 525 nm ($2H_{11/2}$ - $4I_{15/2}$) and 545 nm ($2S_{3/2}$ - $4I_{15/2}$) with a resolution of about 0.5 K.211 Indeed, the sensitivity of UCL materials in temperature sensing

can be improved by the fluorescent resonance energy transfer (FRET) process because of spectral overlapping of UCL emission and absorption of organic dye, as well as superior sensitivity of organic dye over UCL materials. In addition, Chen et al. reported a FRET system composed of NaYF4:Yb/Er as a donor and Rhodamine 6G (R6G) as an acceptor. Since the emitting wavelength at 525–560 nm overlaps with the absorption band of R6G, R6G can emit sharp 575 nm emission (Fig. 17(b)). Fig. 17(c) shows the decrease of UCL emission from NaYF4:Yb/Er upon increasing the concentration of R6G due to increased absorption of R6G. The gradual red shift in the fluorescence of R6G was attributed to the absorption effect. Based on the FRET system, a hemi-spherical microstructure photonic device was prepared and the average temperature sensitivity was estimated to be 1% KÀ1 over the whole physiological temperature range (298–318 K) and 2.7% KÀ1 in the higher temperature region (320–330 K).235

In addition to temperature sensors, Wolfbeis and co-workers reported a pH sensor fabricated by using NaYF4:Yb/Er nanorods and bromothymol blue (BTB). BTB is a non-toxic material that undergoes significant spectral red shift upon changing pH values. The pH dependent absorption and UCL emission of NaYF4:Yb/Er nanorods displayed different amounts of overlapping of UCL emission with the absorption of BTB. Moreover, the pH sensor can work in the range from pH 6 to 10 with excellent reversibility tested in a sensor membrane.138 Recently, Yan et al. presented a reversible pH sensor based on free standing optical hybrid film composed of PEI coated NaYF4:Yb/Er NPs and graphene oxide (GO) (Fig. 18(a)–(e)).137 The pH dependent relationship between theattractionofPEI and GOwas illustrated by isothermal titration calorimetry, in which increased pH rendered more negative charges on GO, enhancing the electrostatic attraction for higher UCL quenching. Fig. 18(f) and (g) show that the UCL emission dropped about 35% at pH 8 compared to pH 5 while the UCL intensity exhibits a linear relationship to pH values. To further confirm the biocompatibility of the pH sensor to biological samples, the hybrid film sensor was tested in the urine of mice and the sensor film displayed a linear relationship over the pH range of 5–8.

5.6 Other potential applications

Counterfeiting of products and documents is a global problem which costs a great deal of money to the government and industries. Anti-fake security application based on UCL is not frequently discussed and reported compared to the biological applications. Recently, UCNCs offer the potential to satisfy the demands for anti-counterfeiting applications because of their small size, low power density NIR excitation, high chemical stability, good wetting properties and compatibility with trans-parent security inks. Kim et al. fabricated photopatternable security ink by synthesizing t-butoxycarbonyl (T-BOC) capped NaYF4:Yb/Er(Tm) UCNCs.199 T-BOC is a photopatternable ligand suitable for the preparation of different patterns via photolitho-graphy in security applications. Importantly, the degree of security can be enhanced by mixing different layers of UCNCs because of multi-color UCL emission. In addition, Lu et al. developed a lifetime encoded document security technique by using
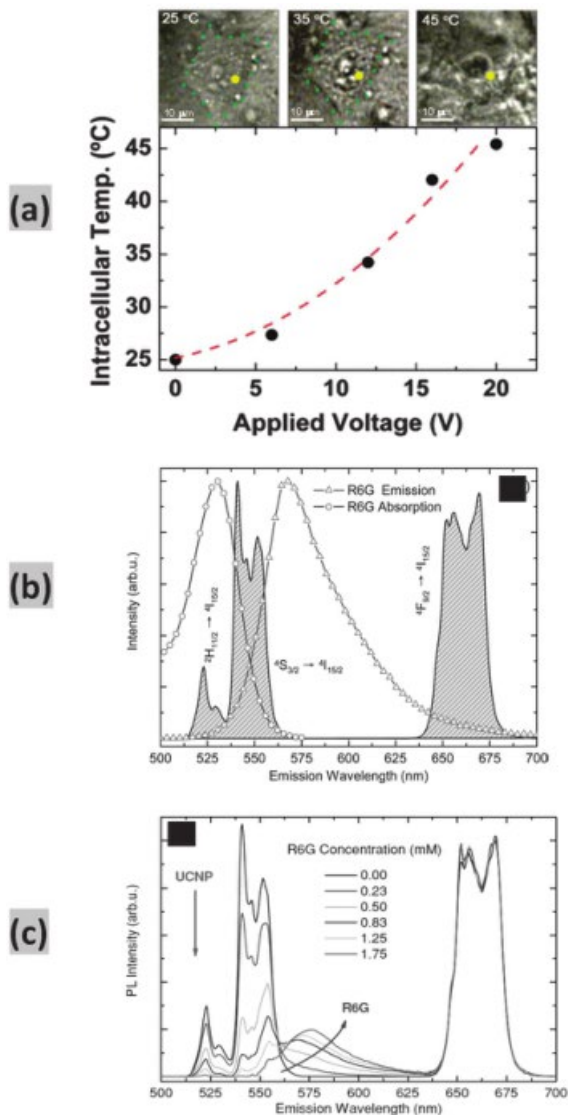
Fig. 17 (a) (top) Optical transmission images of an individual HeLa cell at three inner temperatures. Cell death is observed at 45 1C. (bottom) Temperature of the HeLa cell determined by the Er$_{3+}$ ion fluorescence in the NaYF$_4$:Yb/Er UCNCs as a function of the applied voltage. (b) UCL from NaYF$_4$:Yb/Er UCNCs (filled spectrum) under NIR laser excitation, the absorption and emission from R6G (circle and triangle line). (c) UCL from NaYF$_4$: Yb/Er UCNCs with different R6G concentrations. (Adapted from ref. 212 and 236. Copyright 2010 and 2013, American Chemical Society and Wiley-VCH Verlag GmbH & Co. KGaA, Weinheim. Reproduced with permission.)

luminescent NaYF$_4$:Yb/Tm UCNCs with tunable lifetime.[236] By using the time-resolved scanning technique, the spatially over-lapped patterns can be resolved by the remarkable UCL emis-sion from different layers. Very recently, Meruga et al. reported the direct printing of UCNCs on paper substrates by aerosol jet printing.[237] In their work, different molar concentrations of NaYF$_4$:Yb/Er(Tm) were synthesized and carefully overlapped for multi-color UCL emission, such as red, green, blue (RGB), cyan and magenta (Fig. 19(a)). Moreover, the fabricated sample can be used to generate highly articulated print images that are scalable over a wide range of sizes. Fig. 19(b) shows a printed
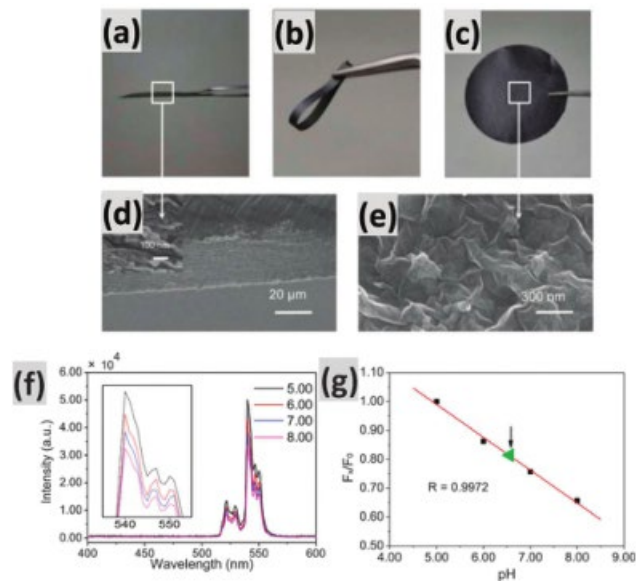

Fig. 18 (a–c) Photographs of the GO-PEI-NaYF$_4$:Yb/Er hybrid film (d) and (e) SEM images of the side view and the surface of the film. (f) UCL spectra of the sensor film as a function of pH upon diode laser excitation at 980 nm. (g) The UCL intensity of the sensor film with F$_x$/F$_0$ plotted against the pH values. The green point is the measured value of F$_x$/F$_0$ of the known B–R buffer solution (pH 6.56). (Adapted from ref. 138. Copyright 2013, Royal Society of Chemistry. Reproduced with permission.)

quick response (QR) code of about 1.5 cm Â 1.5 cm on paper and the corresponding UCL image of the QR code. This example shows that UCNCs are not only capable of qualitative authentication markings, but also of encoding information.

To meet the challenge of expanding counterfeiting, the security printing industry has been undergoing significant changes involving technological complexity from single security ink to multiple-counterfeiting technology. The reason behind the product upgrade is features of security ink. Counterfeiting of a single ink features a single, easy to fabricate and identify, but also easy to imitate and therefore, the fidelity of single security is not strong. According to the principle described in the previous section of this review article, UCL materials can possess magnetic and temperature dependent features besides UCL properties. Therefore, the degree of security should be increased when using the stimuli responsive properties of UCL materials. For instance, the magnetic responsive property grafted by the anchoring of super-paramagnetic IONPs or core–shell designs containing Fe$_3$O$_4$ could be considered to design dual modal security ink. Nowadays, portable and dual modal UV/magnetic testers are very popular, but it seems that there has been no combination of NIR excited UCL/magnetic security technology in the market so far.

In addition, UCNPs have also found practical applications in photocatalysis. Titanium dioxide (TiO$_2$) has been well-known to be an efficient material for photocatalysis so far and the commercialized Degussa P25 with mixed anatase/rutile phase is readily available.[238,239] The upconverted UV photons from NIR in Tm$_{3+}$ doped UCNPs provide the opportunity to enhance the photocatalytic performance because of enhanced electron–hole pair generations.[240] However, recent report indicated that not only
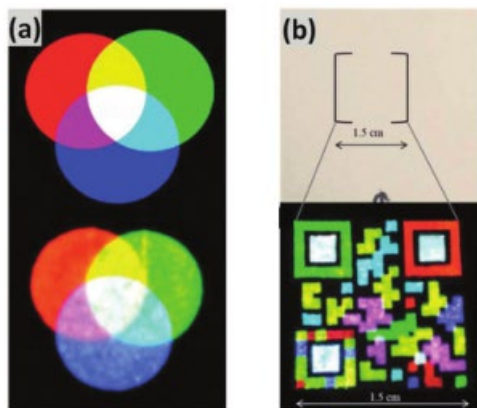
Fig. 19 (a) (top) Schematic representation of the RGB additive color model by primary-color circles producing secondary colors. (bottom) UCL image of RGB overlapping circles printed using the UCNC inks under 980 nm excitation (5 W cmˉ²) producing secondary colors. (b) Paper on which the multi-colored QR code was printed using an aerosol jet printer and the corresponding UCL image of the multi-colored QR code printed using RGB UCNC ink. (Adapted from ref. 238. Copyright 2014, Royal Society of Chemistry. Reproduced with permission.)

Tm^{3+} doped UCNPs are able to enhance photocatalysis is but also Er^{3+} doped UCNPs.[241] Very recently, Wang et al. prepared and used two types of core-double shell $NaYF_4$:Yb/Tm(Er)@SiO_2@TiO_2 UCNPs to compare their photocatalytic performance in the degradation of Rhodamine B.[242] Unlike the previously mentioned example, they have successfully extended the absorption band of TiO_2 from UV to about 828 nm. The improved photocatalytic performance under 980 nm laser irradiation is attributed to efficient energy transfer from the UCNP core to the outer TiO_2 shell.

6. Conclusions and perspectives

This review has comprehensively described the underlying principle and physical mechanisms of the rarely summarized stimuli responses beyond NIR excitations in UCL materials, such as magnetic and electric fields, X-ray, electron beams, temperature and pH. Apart from the magnetization and relaxation, magnetic dependent UCL is due to an increase in the energy gaps between splitting of sub-levels with increasing applied magnetic field. On the other hand, electric field response of UCL materials is attributed to the variation of crystal symmetry in UCL materials under electric field, while the X-ray response is mainly due to the intrinsic X-ray attenuation property of Ln dopants and other heavy elements in UCL materials. Moreover, intense CL emission can be observed when UCL materials are bombarded by the high energy electron beam. Temperature responsive UCL materials are mainly due to the closeness of some energy levels in the activator ions, such as Er^{3+} and Tm^{3+} ions. The close energy levels are readily susceptible to thermal agitation, and therefore the non-radiative transition probabilities are affected in those energy levels. Moreover, the capping ligands, molecules and linkages on the surface of UCL materials are pH sensitive, therefore changes in pH will induce the variation in some characteristics of the surface species, leading to pH response of UCL materials. We have introduced a variety of techniques suitable for the characterization of stimulus response of UCL materials. Interestingly, the designs of UCL materials allow the coupling of single stimulus or multi-stimuli to meet the needs for a range of applications, such as multimodal bioimaging, drug delivery and release, electro-optical modulation, magnetic, temperature, pH sensing and multiple security ink applications. Despite the significant advances of the reported studies, the in-depth fundamental and systematic research studies on the stimulus response of UCL materials are still at the infant stage. Accordingly, we suggest some future development directions for new advancements of this field toward this end.

One significant challenge is to observe sensitive magneto-luminescence. In the future, it is essential to develop high-performance magneto-optical sensors based on UCL materials. Perhaps, one may explore novel designs or methods, such as core–shell structures composed of magnetic layers to enhance the UCL under low magnetic field. Note that Jia et al. recently observed the remnant magnetic field enhanced downconversion luminescence in core–shell $CoFe_2O_4$@YVO_4:Eu^{3+}[243] and $CoFe_2O_4$/SiO_2/Y_2O_3:Eu^{3+}.[244] Regarding electric response of UCL materials, our group's observation of electric field modulated UCL from BTO:Yb/Er just opens up a door for investigating the fundamental mechanism of ferroelectric based UCL materials and raises hopes for their multifunctional applications. Apparently, further studies of the relationship between the UCL modification and ferroelectric properties such as polarizations and domains are highly desired. Furthermore, it would be interesting to find more systems beyond the BTO host and more types beyond thin films which have a similar electric-controlled UCL effect. On the other hand, it is expected that temperature and pH responsive applications will move forward into controlled release agents in biological systems beyond drug delivery and release applications. Lastly, it should be pointed out that the triggers responded by UCL materials should not be restricted to the electric field, the magnetic field, X-ray, the electron beam, temperature and pH which have been discussed in this article. More stimuli such as mechanical stress[245,246] can be considered to couple into UCL materials. Very recently, our group had tuned ultrabroadband NIR luminescence of STO:Ni thin films by using biaxial strain induced by piezoelectric PMN-PT.[247] The proposed strategy can be considered to expand the study of stimuli responsive UCL materials in the future. We hope that this review can provide inspiring ideas to make advances in future in the expanding applications of stimuli responsive UCL materials.

Acknowledgements

References

1 J. Thévenot, H. Oliveira, O. Sandre and S. Lecommandoux, Chem. Soc. Rev., 2013, 42, 7099–7116.
2 E. G. Kelley, J. N. L. Albert, M. O. Sullivan and T. H. Epps, Chem. Soc. Rev., 2013, 42, 7057–7071.

3 M. A. C. Stuart, W. T. S. Huck, J. Genzer, M. Mu¨ller, C. Ober, M. Stamm, G. B. Sukhorukov, I. Szleifer, V. V. Tsukruk, M. Urban, F. Winnik, S. Zauscher, I. Luzinov and S. Minko, Nat. Mater., 2010, 9, 101–113.

4 P. Theato, B. S. Sumerlin, R. K. O'Reilly and T. H. Epps, Chem. Soc. Rev., 2013, 42, 7055–7056.

5 M. Chorny, I. Fishbein, B. B. Yellen, I. S. Alferiev, M. Bakay, S. Ganta, R. Adamo, M. Amiji, G. Friedman and R. J. Levy, Proc. Natl. Acad. Sci. U. S. A., 2010, 107, 8346–8351.

6 U. N. Kumar, K. Kratz, M. Heuchel, M. Behl and A. Lendlein, Adv. Mater., 2011, 23, 4157–4162.

7 Y. Amamoto, J. Kamada, H. Otsuka, A. Takahara and K. Matyjaszewski, Angew. Chem., Int. Ed., 2011, 50, 1660–1663.

8 F. Auzel, Chem. Rev., 2004, 104, 139–173.

9 M. Haase and H. Scha¨fer, Angew. Chem., Int. Ed., 2011, 50, 5808–5829.

10 G. Chen, H. Qiu, P. N. Prasad and X. Chen, Chem. Rev., 2014, 114, 5161–5214.

11 J. Zhou, Z. Liu and F. Li, Chem. Soc. Rev., 2012, 41, 1323–1349.

12 X. Huang, S. Han, W. Huang and X. Liu, Chem. Soc. Rev., 2013, 42, 173–201.

13 Y. Liu, D. Tu, H. Zhu, E. Ma and X. Chen, Nanoscale, 2013, 5, 1369–1384.

14 F. Wang and X. Liu, Chem. Soc. Rev., 2009, 38, 976–989.

15 F. Wang, R. Deng, J. Wang, Q. Wang, Y. Han, H. Zhu, X. Chen and X. Liu, Nat. Mater., 2011, 10, 968–973.

16 F. Zhang, G. B. Braun, Y. Shi, Y. Zhang, X. Sun, N. O. Reich, D. Zhao and G. Stucky, J. Am. Chem. Soc., 2010, 132, 2850–2851.

17 X. Chen, E. Ma and G. Liu, J. Phys. Chem. C, 2007, 10404–10411.

18 A. Patra and C. Friend, J. Phys. Chem. B, 2002, 10, 1909–1912.

19 A. S. S. de Camargo, J. F. Possatto, L. A. D. O. Nunes, E´. R. Botero, E´. R. M. Andreeta, D. Garcia and J. A. Eiras, Solid State Commun., 2006, 137, 1–5.

20 Z. P. Cai and H. Y. Xu, Sens. Actuators, A, 2003, 108, 187–192.

21 G. Y. Tan, X. Yang and S. Xiao, Phys. B, 2011, 406, 3475–3478.

22 Y. Zhang, J. Hao, C. L. Mak and X. Wei, Opt. Express, 2011, 19, 1824–1829.

23 G. Tripathi, V. K. Rai and S. B. Rai, Opt. Mater., 2007, 30, 201–206.

24 G. Y. Chen, H. C. Liu, G. Somesfalean, Y. Q. Sheng, H. J. Liang, Z. G. Zhang, Q. Sun and F. P. Wang, Appl. Phys. Lett., 2008, 92, 113114.

25 X. Wu and K. W. Kwok, J. Am. Ceram. Soc., 2014, 7, 1–7.

26 X. Wu, K. W. Kwok and F. Li, J. Alloys Compd., 2013, 580, 88–92.

27 Q. Lu, Y. Hou, A. Tang, X. Liu and F. Teng, Mater. Lett., 2013, 99, 115–117.

28 G. Chen, T. Y. Ohulchanskyy, A. Kachynski, H. Agren and P. N. Prasad, ACS Nano, 2011, 5, 4981–4986.

29 Z. Li and Y. Zhang, Angew. Chem., Int. Ed., 2006, 118, 7896–7899.

30 J.-C. Zhou, Z.-L. Yang, W. Dong, R.-J. Tang, L.-D. Sun and C.-H. Yan, Biomaterials, 2011, 32, 9059–9067.

31 L. Xiong, T. Yang, Y. Yang, C. Xu and F. Li, Biomaterials, 2010, 31, 7078–7085.

32 Q. Liu, Y. Sun, T. Yang, W. Feng, C. Li and F. Li, J. Am. Chem. Soc., 2011, 133, 17122–17125.

33 W. Niu, S. Wu, S. Zhang and L. Li, Chem. Commun., 2010, 46, 3908–3910.

34 J. Wang, F. Wang, J. Xu, Y. Wang, Y. Liu, X. Chen, H. Chen and X. Liu, C. R. Chim., 2010, 13, 731–736.

35 C. Li, Z. Quan, J. Yang, P. Yang and J. Lin, Inorg. Chem., 2007, 46, 6329–6337.

36 N. Niu, P. Yang, H. Fei, X. Zhang, S. Gai, C. Li and J. Lin, J. Mater. Chem., 2012, 22, 10889–10899.

37 Z.-L. Wang, J. Hao, H. L. W. Chan, W.-T. Wong and K.-L. Wong, Small, 2012, 8, 1863–1868.

38 S. Zeng, J. Xiao, Q. Yang and J. Hao, J. Mater. Chem., 2012, 22, 9870–9874.

39 F. Wang and X. Liu, J. Am. Chem. Soc., 2008, 130, 5642–5643.

40 J. Wang, F. Wang, C. Wang, Z. Liu and X. Liu, Angew. Chem., Int. Ed., 2011, 50, 10369–10372.

41 N. Liu, W. Qin, G. Qin, T. Jiang and D. Zhao, Chem. Commun., 2011, 47, 7671–7673.

42 R. Naccache, F. Vetrone, V. Mahalingam, L. A. Cuccia and J. A. Capobianco, Chem. Mater., 2009, 717–723.

43 F. Vetrone, V. Mahalingam and J. A. Capobianco, Chem. Mater., 2009, 21, 1847–1851.

44 N. J. J. Johnson, N. M. Sangeetha, J.-C. Boyer and F. C. J. M. van Veggel, Nanoscale, 2010, 2, 771–777.

45 J.-C. Boyer, F. Vetrone, L. A. Cuccia and J. A. Capobianco, J. Am. Chem. Soc., 2006, 128, 7444–7445.

46 G. Ren, S. Zeng and J. Hao, J. Phys. Chem. C, 2011, 115, 20141–20147.

47 H.-T. Wong, F. Vetrone, R. Naccache, H. L. W. Chan, J. Hao and J. A. Capobianco, J. Mater. Chem., 2011, 21, 16589–16596.

48 M.-K. Tsang, S. Zeng, H. L. W. Chan and J. Hao, Opt. Mater., 2013, 35, 2691–2697.

49 Z.-L. Wang, J. H. Hao and H. L. W. Chan, J. Mater. Chem., 2010, 20, 3178–3185.

50 J.-H. Zeng, J. Su, Z.-H. Li, R.-X. Yan and Y.-D. Li, Adv. Mater., 2005, 17, 2119–2123.

51 Q. Zheng, H. Zhu, S. Chen, C. Tang and X. Chen, Nat. Photonics, 2013, 7, 234–239.

52 P. Ptacek, H. Scha¨fer, K. Ko¨mpe and M. Haase, Adv. Funct. Mater., 2007, 17, 3843–3848.

53 C. Liu, H. Wang, X. Zhang and D. Chen, J. Mater. Chem., 2009, 19, 489–496.

54 F. He, N. Niu, L. Wang, J. Xu, Y. Wang, G. Yang, S. Gai and P. Yang, Dalton Trans., 2013, 42, 10019–10028.

55 H. Chen, B. Qi, T. Moore, D. C. Colvin, T. Crawford, J. C. Gore, F. Alexis, O. T. Mefford and J. N. Anker, Small, 2014, 10, 160–168.

56 S. Liu, G. Chen, T. Y. Ohulchanskyy, M. T. Swihart and P. N. Prasad, Theranostics, 2013, 3, 275–281.

57 Z. Xu, C. Li, D. Yang, W. Wang, X. Kang, M. Shang and J. Lin, Phys. Chem. Chem. Phys., 2010, 12, 11315–11324.

58 C. Xu, M. Ma, L. Yang, S. Zeng and Q. Yang, J. Lumin., 2011, 131, 2544–2549.

59 S. Zeng, M.-K. Tsang, C.-F. Chan, K.-L. Wong, B. Fei and J. Hao, Nanoscale, 2012, 4, 5118–5124.

60 S. Zeng, M.-K. Tsang, C.-F. Chan, K.-L. Wong and J. Hao, Biomaterials, 2012, 33, 9232–9238.

61 D. Yang, C. Li, G. Li, M. Shang, X. Kang and J. Lin, J. Mater. Chem., 2011, 21, 5923–5927.

62 H.-T. Wong, H. L. W. Chan and J. H. Hao, Appl. Phys. Lett., 2009, 95, 022512.

63 F. Evanics and P. Diamente, Chem. Mater., 2006, 18, 2499–2505.

64 S. Wang, S. Su, S. Song, R. Deng and H. Zhang, CrystEngComm, 2012, 14, 4266–4269.

65 D. Yang, G. Li, X. Kang, Z. Cheng, P. Ma, C. Peng, H. Lian, C. Li and J. Lin, Nanoscale, 2012, 4, 3450–3459.

66 H.-T. Wong, M.-K. Tsang, C.-F. Chan, K.-L. Wong, B. Fei and J. Hao, Nanoscale, 2013, 5, 3465–3473.

67 Q. Ju, D. Tu, Y. Liu, R. Li, H. Zhu, J. Chen, Z. Chen, M. Huang and X. Chen, J. Am. Chem. Soc., 2012, 134, 1323–1330.

68 J. Hao, Y. Zhang and X. Wei, Angew. Chem., Int. Ed., 2011, 50, 6876–6880.

69 Y. Zhang and J. Hao, J. Appl. Phys., 2013, 113, 184112.

70 Q. Sun, X. Chen, Z. Liu, F. Wang, Z. Jiang and C. Wang, J. Alloys Compd., 2011, 509, 5336–5340.

71 F. Gao, G. Wu, H. Zhou and D. Bao, J. Appl. Phys., 2009, 106, 126104.

72 N. Lee, S. H. Choi and T. Hyeon, Adv. Mater., 2013, 25, 2641–2660.

73 G. Wang, Q. Peng and Y. Li, Acc. Chem. Res., 2011, 44, 322–332.

74 W. Feng, C. Han and F. Li, Adv. Mater., 2013, 25, 5287–5303.

75 Y. Liu, D. Tu, H. Zhu and X. Chen, Chem. Soc. Rev., 2013, 42, 6924–6958.

76 S. Wang, J. Feng, S. Song and H. Zhang, CrystEngComm, 2013, 15, 7142–7151.

77 C. Li and J. Lin, J. Mater. Chem., 2010, 20, 6831–6847.

78 M. Wang, G. Abbineni, A. Clevenger, C. Mao and S. Xu, Nanomedicine, 2011, 7, 710–729.

79 Y. Yang, Microchim. Acta, 2013, 181, 263–294.

80 P. Qiu, N. Zhou, H. Chen, C. Zhang, G. Gao and D. Cui, Nanoscale, 2013, 5, 11512–11525.

81 L. Cheng, C. Wang and Z. Liu, Nanoscale, 2013, 5, 23–37.

82 W. Feng, X. Zhu and F. Li, NPG Asia Mater., 2013, 5, e75.

83 J. Chen and J. X. Zhao, Sensors, 2012, 12, 2414–2435.

84 F. Wang, D. Banerjee, Y. Liu, X. Chen and X. Liu, Analyst, 2010, 135, 1839–1854.

85 Z. Gu, L. Yan, G. Tian, S. Li, Z. Chai and Y. Zhao, Adv. Mater., 2013, 25, 3758–3779.

86 S. Gai, C. Li, P. Yang and J. Lin, Chem. Rev., 2014, 114, 2343–2389.

87 Y. Zhang and J. Hao, J. Mater. Chem. C, 2013, 1, 5607–5618.

88 B. M. van der Ende, L. Aarts and A. Meijerink, Phys. Chem. Chem. Phys., 2009, 11, 11081–11095.

89 F. Wang and X. Liu, Acc. Chem. Res., 2014, 47, 1378–1385.

90 J. Wilson and J. Hawkes, Optoelectronics: an introduction, Prentice Hall PTR, New York, Toronto, 3rd edn, 1998.

91 H. Ebert, Rep. Prog. Phys., 1996, 59, 1665–1735.

92 C. V. Dewitz, F. Hatami, M. Millot, J. M. Broto, J. Le´otin and W. T. Masselink, Appl. Phys. Lett., 2009, 95, 151105.

93 M. Cardona, T. Ruf, S. I. Gubarev and K. Ploog, Solid State Commun., 1993, 85, 853–857.

94 N. Ko¨che, F. Plentz, W. N. Rodrigues, M. V. B. Moreira, A. G. De Oliveira and J. C. Gonza, Phys. B, 2001, 298, 295–301.

95 M. Hayne and B. Bansal, Luminescence, 2012, 27, 179–196.

96 J. Mezyk, R. Tubino, A. Monguzzi, A. Mech and F. Meinardi, Phys. Rev. Lett., 2009, 102, 087404.

97 Y. Liu, D. Wang, J. Shi, Q. Peng and Y. Li, Angew. Chem., Int. Ed., 2013, 52, 4366–4369.

98 V. K. Tikhomirov, L. F. Chibotaru, D. Saurel, P. Gredin, M. Mortier and V. V. Moshchalkov, Nano Lett., 2009, 9, 721–724.

99 S. K. Singh, K. Kumar, M. K. Srivastava, D. K. Rai and S. B. Rai, Opt. Lett., 2010, 35, 1575–1577.

100 G. Blasse and B. C. Grabmaier, Luminescent Materials, Springer, Berlin, 1994.

101 B. R. Judd, Phys. Rev., 1962, 197, 750–761.

102 M. J. Weber, Phys. Rev., 1967, 157, 262–272.

103 J. H. Hubbell and S. M. Seltzer, Natl. Inst. Stand. Technol., 1996, http://physics.nist.gov/PhysRefData/XrayMassCoef/.

104 K. Smits, D. Millers, L. Grigorjeva, J. D. Fidelus and W. Lojkowski, J. Phys.: Conf. Ser., 2007, 93, 012035.

105 M. Shang, D. Geng, Y. Zhang, G. Li, D. Yang, X. Kang and J. Lin, J. Mater. Chem., 2012, 22, 19094–19104.

106 J. Hao, J. Gao and M. Cocivera, Appl. Phys. Lett., 2003, 82, 2224–2226.

107 J. Hao and M. Cocivera, Appl. Phys. Lett., 2001, 79, 740–742.

108 J. H. Hao and J. Gao, Appl. Phys. Lett., 2004, 85, 3720–3722.

109 J. Hao, J. Gao and M. Cocivera, Appl. Phys. Lett., 2003, 82, 2778–2780.

110 J. Wang, J. H. Hao and P. A. Tanner, Opt. Express, 2011, 19, 11753–11758.

111 C. Feldman, Phys. Rev., 1960, 117, 455–459.

112 W. Yu, W. Xu, H. Song and S. Zhang, Dalton Trans., 2014, 43, 6139–6147.

113 A. M. Pires, O. A. Serra, S. Heer and H. U. Gudel, J. Appl. Phys., 2005, 98, 063529.

114 S. Shionoya, W. M. Yen and H. Yamamoto, Phosphor handbook, CRC Press, Boca Raton, FL, 2006.

115 H. Berthou and C. K. Jo¨rgensen, Opt. Lett., 1990, 15, 1100–1102.

116 S. Zhou, K. Deng, X. Wei, G. Jiang, C. Duan, Y. Chen and M. Yin, Opt. Commun., 2013, 291, 138–142.

117 X. Wang, O. S. Wolfbeis and R. J. Meier, Chem. Soc. Rev., 2013, 42, 7834–7869.

118 E. Sar¨di, B. Samson, L. Aigouy, S. Volz, P. Lo¨w, C. Bergaud and M. Mortier, Nanotechnology, 2009, 20, 115703.

119 N. Bogdan, F. Vetrone, G. A. Ozin and J. A. Capobianco, Nano Lett., 2011, 11, 835–840.

120 S.-Z. Zhang, L.-D. Sun, H. Tian, Y. Liu, J.-F. Wang and C.-H. Yan, Chem. Commun., 2009, 2547–2549.

121 D. R. Lide, CRC handbook of chemistry and physics, CRC Press, Boca Raton, FL, 2005, pp. 143–148.

122 G. Tian, Z. Gu, L. Zhou, W. Yin, X. Liu, L. Yan, S. Jin, W. Ren, G. Xing, S. Li and Y. Zhao, Adv. Mater., 2012, 24, 1226–1231.

123 S. Zeng, Z. Yi, W. Lu, C. Qian, H. Wang, L. Rao, T. Zeng, H. Liu, H. Liu, B. Fei and J. Hao, Adv. Funct. Mater., 2014, 24, 4051–4059.

124 J. Shen, L.-D. Sun, Y.-W. Zhang and C.-H. Yan, Chem. Commun., 2010, 46, 5731–5733.

125 C. Zhong, P. Yang, X. Li, C. Li, D. Wang, S. Gai and J. Lin, RSC Adv., 2012, 2, 3194–3197.

126 L. Zeng, L. Xiang, W. Ren, J. Zheng, T. Li, B. Chen, J. Zhang, C. Mao, A. Li and A. Wu, RSC Adv., 2013, 3, 13915–13925.

127 L. Zhang, Y.-S. Wang, Y. Yang, F. Zhang, W.-F. Dong, S.-Y. Zhou, W.-H. Pei, H.-D. Chen and H.-B. Sun, Chem. Commun., 2012, 48, 11238–11240.

128 H. Xing, W. Bu, S. Zhang, X. Zheng, M. Li, F. Chen, Q. He, L. Zhou, W. Peng, Y. Hua and J. Shi, Biomaterials, 2012, 33, 1079–1089.

129 K. S. Soppimath, D. C.-W. Tan and Y.-Y. Yang, Adv. Mater., 2005, 17, 318–323.

130 M. S. Yavuz, Y. Cheng, J. Chen, C. M. Cobley, Q. Zhang, M. Rycenga, J. Xie, C. Kim, K. H. Song, A. G. Schwartz, L. V. Wang and Y. Xia, Nat. Mater., 2009, 8, 935–939.

131 B. Chang, X. Sha, J. Guo, Y. Jiao, C. Wang and W. Yang, J. Mater. Chem., 2011, 21, 9239–9247.

132 D. Yang, P. Ma, Z. Hou, Z. Cheng, C. Li and J. Lin, Chem. Soc. Rev., 2014, DOI: 10.1039/c4cs00155a.

133 L. Chen, L. Li, L. Zhang, S. Xing, T. Wang, Y. A. Wang, C. Wang and Z. Su, ACS Appl. Mater. Interfaces, 2013, 5, 7282–7290.

134 L. Li, C. Liu, L. Zhang, T. Wang, H. Yu, C. Wang and Z. Su, Nanoscale, 2013, 5, 2249–2253.

135 X. Jia, J. Yin, D. He, X. He, K. Wang, M. Chen and Y. Li, J. Biomed. Nanotechnol., 2013, 9, 2063–2072.

136 C. Wang, L. Cheng, Y. Liu, X. Wang, X. Ma, Z. Deng, Y. Li and Z. Liu, Adv. Funct. Mater., 2013, 23, 3077–3086.

137 L. Yan, Y.-N. Chang, W. Yin, X. Liu, D. Xiao, G. Xing, L. Zhao, Z. Gu and Y. Zhao, Phys. Chem. Chem. Phys., 2014, 16, 1576–1582.

138 L.-N. Sun, H. Peng, M. I. J. Stich, D. Achatz and O. S. Wolfbeis, Chem. Commun., 2009, 5000–5002.

139 J. W. Stouwdam and F. C. J. M. van Veggel, Nano Lett., 2002, 2, 733–737.

140 S. Heer, K. Kompe, H.-U. Gudel and M. Haase, Adv. Mater., 2004, 16, 2102–2105.

141 G. Yi, H. Lu, S. Zhao, Y. Ge and W. Yang, Nano Lett., 2004, 4, 2191–2196.

142 A. Xia, Y. Gao, J. Zhou, C. Li, T. Yang, D. Wu, L. Wu and F. Li, Biomaterials, 2011, 32, 7200–7208.

143 Y. Il Park, J. H. Kim, K. T. Lee, K.-S. Jeon, H. Bin Na, J. H. Yu, H. M. Kim, N. Lee, S. H. Choi, S.-I. Baik, H. Kim, S. P. Park, B.-J. Park, Y. W. Kim, S. H. Lee, S.-Y. Yoon, I. C. Song, W. K. Moon, Y. D. Suh and T. Hyeon, Adv. Mater., 2009, 21, 4467–4471.

144 P. Ma, H. Xiao, X. Li, C. Li, Y. Dai, Z. Cheng, X. Jing and J. Lin, Adv. Mater., 2013, 25, 4898–4905.

145 Z. Yi, G. Ren, L. Rao, H. Wang, H. Liu and S. Zeng, J. Alloys Compd., 2014, 589, 502–506.

146 H. Liu, W. Lu, H. Wang, L. Rao, Z. Yi, S. Zeng and J. Hao, Nanoscale, 2013, 5, 6023–6029.

147 T. Cao, Y. Yang, Y. Gao, J. Zhou, Z. Li and F. Li, Biomaterials, 2011, 32, 2959–2968.

148 A. Patra, C. S. Friend, R. Kapoor and P. N. Prasad, Chem. Mater., 2003, 15, 3650–3655.

149 C. Dong and F. C. J. M. van Veggel, ACS Nano, 2009, 3, 123–130.

150 X. Qin, T. Yokomori and Y. Ju, Appl. Phys. Lett., 2007, 90, 073104.

151 X. Qin, Y. Ju, S. Bernhard and N. Yao, J. Mater. Res., 2011, 20, 2960–2968.

152 X. Luo and W. Cao, J. Alloys Compd., 2008, 460, 529–534.

153 G.-S. Yi and G.-M. Chow, J. Mater. Chem., 2005, 15, 4460–4464.

154 S. Heer, O. Lehmann, M. Haase and H.-U. Gu¨del, Angew. Chem., Int. Ed., 2003, 42, 3179–3182.

155 X. Wang, J. Zhuang, Q. Peng and Y. Li, Nature, 2005, 437, 121–124.

156 F. Wang, Y. Han, C. S. Lim, Y. Lu, J. Wang, J. Xu, H. Chen, C. Zhang, M. Hong and X. Liu, Nature, 2010, 463, 1061–1065.

157 F. Zhang, Y. Wan, T. Yu, F. Zhang, Y. Shi, S. Xie, Y. Li, L. Xu, B. Tu and D. Zhao, Angew. Chem., Int. Ed., 2007, 46, 7976–7979.

158 D. Chen, P. Huang, Y. Yu, F. Huang, A. Yang and Y. Wang, Chem. Commun., 2011, 47, 5801–5803.

159 J. Zhou, G. Chen, E. Wu, G. Bi, B. Wu, Y. Teng, S. Zhou and J. Qiu, Nano Lett., 2013, 13, 2241–2246.

160 J. Zhou, M. Yu, Y. Sun, X. Zhang, X. Zhu, Z. Wu, D. Wu and F. Li, Biomaterials, 2011, 32, 1148–1156.

161 L. Wang, P. Li and Y. Li, Adv. Mater., 2007, 19, 3304–3307.

162 L. W. Yang, Y. Li, Y. C. Li, J. J. Li, J. H. Hao, J. X. Zhong and P. K. Chu, J. Mater. Chem., 2012, 22, 2254–2262.

163 L. Yang, Y. Li, S. Yu, J. Hao, J. Zhong and P. K. Chu, Chem. Commun., 2011, 47, 12544–12546.

164 D. Wang, L. Ren, X. Zhou, X.-Z. Wang, J. Zhou, Y. Han and N. Kang, Nanotechnology, 2012, 23, 225705.

165 S. Zeng, H. Wang, W. Lu, Z. Yi, L. Rao, H. Liu and J. Hao, Biomaterials, 2014, 35, 2934–2941.

166 D. Chen, Y. Yu, F. Huang and Y. Wang, Chem. Commun., 2011, 47, 2601–2603.

167 H. Hu, Z. Chen, T. Cao, Q. Zhang, M. Yu, F. Li, T. Yi and C. Huang, Nanotechnology, 2008, 19, 375702.

168 X. Bai, D. Li, Q. Liu, B. Dong, S. Xu and H. Song, J. Mater. Chem., 2012, 22, 24698–24704.

169 T. Xie, S. Li, Q. Peng and Y. Li, Angew. Chem., Int. Ed., 2009, 48, 196–200.

170 C. Xu, M. Ma, L. Yang, S. Zeng and Q. Yang, J. Colloid Interface Sci., 2012, 368, 49–55.

171 S. Zeng, G. Ren, W. Li, C. Xu and Q. Yang, J. Phys. Chem. C, 2010, 3, 10750–10754.

172 H. Wang, Z. Yi, L. Rao, H. Liu and S. Zeng, J. Mater. Chem. C, 2013, 1, 5520–5526.

173 S. Zeng, G. Ren, C. Xu and Q. Yang, CrystEngComm, 2011, 13, 1384–1390.

174 Z.-L. Wang, J. Hao, H. L. W. Chan, G.-L. Law, W.-T. Wong, K.-L. Wong, M. B. Murphy, T. Su, Z. H. Zhang and S. Q. Zeng, Nanoscale, 2011, 3, 2175–2181.

175 W. W. Ye, M.-K. Tsang, X. Liu, M. Yang and J. Hao, Small, 2014, 10, 2390–2397.

176 Y.-W. Zhang, X. Sun, R. Si, L.-P. You and C.-H. Yan, J. Am. Chem. Soc., 2005, 127, 3260–3261.

177 J. Boyer, L. A. Cuccia and J. A. Capobianco, Nano Lett., 2007, 7, 847–852.

178 J. Ryu, H. Park, K. Kim, H. Kim, J. H. Yoo, M. Kang, K. Im, R. Grailhe and R. Song, J. Phys. Chem. C, 2010, 114, 21077–21082.

179 H. Xing, S. Zhang, W. Bu, X. Zheng, L. Wang, Q. Xiao, D. Ni, J. Zhang, L. Zhou, W. Peng, K. Zhao, Y. Hua and J. Shi, Adv. Mater., 2014, 26, 3867–3872.

180 F. Wang, R. Deng and X. Liu, Nat. Protoc., 2014, 9, 1634–1644.

181 Y. Ai, D. Tu, W. Zheng, Y. Liu, J. Kong, P. Hu, Z. Chen, M. Huang and X. Chen, Nanoscale, 2013, 5, 6430–6438.

182 X. Teng, Y. Zhu, W. Wei, S. Wang, J. Huang, W. Hu, L. Y. A. Tok, Y. Han, Q. Zhang, Q. Fan, W. Huang, J. A. Capobianco and L. Huang, J. Am. Chem. Soc., 2012, 134, 8340–8343.

183 J. Peng, Y. Sun, L. Zhao, Y. Wu, W. Feng, Y. Gao and F. Li, Biomaterials, 2013, 34, 9535–9544.

184 A. Xia, M. Chen, Y. Gao, D. Wu, W. Feng and F. Li, Biomaterials, 2012, 33, 5394–5405.

185 L. P. Qian, L. H. Zhou, H.-P. Too and G.-M. Chow, J. Nanopart. Res., 2010, 13, 499–510.

186 G. Yi and G. Chow, Chem. Mater., 2007, 298, 341–343.

187 H. Mai, Y. Zhang, L.-D. Sun and C.-H. Yan, J. Phys. Chem. C, 2007, 111, 13721–13729.

188 F. Vetrone, R. Naccache, V. Mahalingam, C. G. Morgan and J. A. Capobianco, Adv. Funct. Mater., 2009, 19, 2924–2929.

189 K. A. Abel, J.-C. Boyer and F. C. J. M. van Veggel, J. Am. Chem. Soc., 2009, 131, 14644–14645.

190 F. Wang, J. Wang and X. Liu, Angew. Chem., Int. Ed., 2010, 49, 7456–7460.

191 Y. Liu, D. Tu, H. Zhu, R. Li, W. Luo and X. Chen, Adv. Mater., 2010, 22, 3266–3271.

192 A. Priyam, N. M. Idris and Y. Zhang, J. Mater. Chem., 2012, 22, 960–965.

193 H. Zhang, Y. Li, I. A. Ivanov, Y. Qu, Y. Huang and X. Duan, Angew. Chem., Int. Ed., 2010, 122, 2927–2930.

194 L. Cheng, K. Yang, Y. Li, X. Zeng, M. Shao, S.-T. Lee and Z. Liu, Biomaterials, 2012, 33, 2215–2222.

195 T. Blumenthal, J. Meruga, P. Stanley May, J. Kellar, W. Cross, K. Ankireddy, S. Vunnam and Q. N. Luu, Nanotechnology, 2012, 23, 185305.

196 L. Xie, Y. Qin and H.-Y. Chen, Anal. Chem., 2012, 84, 1969–1974.

197 C. Lin, M. T. Berry, R. Anderson, S. Smith and P. S. May, Chem. Mater., 2009, 21, 3406–3413.

198 S. Sivakumar, F. C. J. M. van Veggel and M. Raudsepp, J. Am. Chem. Soc., 2005, 127, 12464–12465.

199 W. J. Kim, M. Nyk and P. N. Prasad, Nanotechnology, 2009, 20, 185301.

200 G. Qin, J. Lu, J. F. Bisson, Y. Feng, K. Ueda, H. Yagi and T. Yanagitani, Solid State Commun., 2004, 132, 103–106.

201 G. Bai, L. Tao, Y. Wang and Y. H. Tsang, Integr. Ferroelectr., 2013, 142, 31–36.

202 C. Ba, L. Nanocrystals, X. Fan, J. Wang, X. Qiao, M. Wang and J. Adam, J. Phys. Chem. B, 2006, 110, 5950–5954.

203 F. Liu, Y. Wang, D. Chen, Y. Yu, E. Ma, L. Zhou and P. Huang, Mater. Lett., 2007, 61, 5022–5025.

204 J. Wang, J. H. Hao and P. A. Tanner, Opt. Lett., 2010, 35, 3922–3924.

205 A. K. Singh, S. K. Singh, B. K. Gupta, R. Prakash and S. B. Rai, Dalton Trans., 2013, 42, 1065–1072.

206 A. Sayoud, J. P. Jouart, N. Trannoy, M. Diaf and T. Duvaut, J. Lumin., 2012, 132, 566–569.

207 B. Dong, B. Cao, Y. He, Z. Liu, Z. Li and Z. Feng, Adv. Mater., 2012, 24, 1987–1993.

208 K. Wu, J. Cui, X. Kong and Y. Wang, J. Appl. Phys., 2011, 110, 053510.

209 R. Martı́n-Rodrı́guez, R. Valiente, F. Rodrı́guez, F. Piccinelli, A. Speghini and M. Bettinelli, Phys. Rev. B: Condens. Matter Mater. Phys., 2010, 82, 075117.

210 K. Zheng, D. Zhao, D. Zhang, N. Liu and W. Qin, J. Fluorine Chem., 2011, 132, 5–8.

211 F. Vetrone, R. Naccache, A. Zamarro´n, A. Juarranz de la Fuente, F. Sanz-Rodrı́guez, L. Martinez Maestro, E. Martı́n Rodriguez, D. Jaque, J. Garcı́a Sole´ and J. A. Capobianco, ACS Nano, 2010, 4, 3254–3258.

212 C. Liu, Z. Gao, J. Zeng, Y. Hou, F. Fang, Y. Li, R. Qiao and L. Shen, ACS Nano, 2013, 7, 7227–7240.

213 J. Zhou, Y. Sun, X. Du, L. Xiong, H. Hu and F. Li, Biomaterials, 2010, 31, 3287–3295.

214 R. Kumar, M. Nyk, T. Y. Ohulchanskyy, C. A. Flask and P. N. Prasad, Adv. Funct. Mater., 2009, 19, 853–859.

215 F. Chen, W. Bu, S. Zhang, X. Liu, J. Liu, H. Xing, Q. Xiao, L. Zhou, W. Peng, L. Wang and J. Shi, Adv. Funct. Mater., 2011, 21, 4285–4294.

216 H. Guo, Z. Li, H. Qian, Y. Hu and I. N. Muhammad, Nanotechnology, 2010, 21, 125602.

217 W. Fan, B. Shen, W. Bu, F. Chen, K. Zhao, S. Zhang, L. Zhou, W. Peng, Q. Xiao, H. Xing, J. Liu, D. Ni, Q. He and J. Shi, J. Am. Chem. Soc., 2013, 135, 6494–6503.

218 G. Chen, T. Y. Ohulchanskyy, W. C. Law, H. Ågren and P. N. Prasad, Nanoscale, 2011, 3, 2003–2008.

219 M. He, P. Huang, C. Zhang, H. Hu, C. Bao, G. Gao, R. He and D. Cui, Adv. Funct. Mater., 2011, 21, 4470–4477.

220 H. Xing, W. Bu, Q. Ren, X. Zheng, M. Li, S. Zhang, H. Qu, Z. Wang, Y. Hua, K. Zhao, L. Zhou, W. Peng and J. Shi, Biomaterials, 2012, 33, 5384–5393.

221 G. Zhang, Y. Liu, Q. Yuan, C. Zong, J. Liu and L. Lu, Nanoscale, 2011, 3, 4365–4371.

222 H. Xing, X. Zheng, Q. Ren, W. Bu, W. Ge, Q. Xiao, S. Zhang, C. Wei, H. Qu, Z. Wang, Y. Hua, L. Zhou, W. Peng, K. Zhao and J. Shi, Sci. Rep., 2013, 3, 1751–1759.

223 Y. Sun, M. Yu, S. Liang, Y. Zhang, C. Li, T. Mou, W. Yang, X. Zhang, B. Li, C. Huang and F. Li, Biomaterials, 2011, 32, 2999–3007.

224 Q. Liu, Y. Sun, C. Li, J. Zhou, C. Li, T. Yang, X. Zhang and T. Yi, ACS Nano, 2011, 5, 3146–3157.

225 Y. Sun, X. Zhu, J. Peng and F. Li, ACS Nano, 2013, 7, 11290–11300.

226 J. Zhang, Z.-F. Yuan, Y. Wang, W.-H. Chen, G.-F. Luo, S.-X. Cheng, R.-X. Zhuo and X.-Z. Zhang, J. Am. Chem. Soc., 2013, 135, 5068–5073.

227 K. K. Cotı′, M. E. Belowich, M. Liong, M. W. Ambrogio, Y. a. Lau, H. a. Khatib, J. I. Zink, N. M. Khashab and J. F. Stoddart, Nanoscale, 2009, 1, 16–39.

228 Y. Yang, Q. Shao, R. Deng, C. Wang, X. Teng, K. Cheng, Z. Cheng, L. Huang, Z. Liu, X. Liu and B. Xing, Angew. Chem., Int. Ed., 2012, 51, 3125–3129.

229 Y. Yang, F. Liu, X. Liu and B. Xing, Nanoscale, 2013, 5, 231–238.

230 M. K. G. Jayakumar, N. M. Idris and Y. Zhang, Proc. Natl. Acad. Sci. U. S. A., 2012, 109, 8483–8488.

231 Y. Yang, B. Velmurugan, X. Liu and B. Xing, Small, 2013, 9, 2937–2944.

232 Y. Chen, K. Ai, Y. Liu and L. Lu, ACS Appl. Mater. Interfaces, 2014, 6, 655–663.

233 X. Zhang, P. Yang, Y. Dai, P. Ma, X. Li, Z. Cheng, Z. Hou, X. Kang, C. Li and J. Lin, Adv. Funct. Mater., 2013, 23, 4067–4078.

234 S. Schietinger, T. Aichele, H.-Q. Wang, T. Nann and O. Benson, Nano Lett., 2010, 10, 134–138.

235 R. Chen, V. D. Ta, F. Xiao, Q. Zhang and H. Sun, Small, 2013, 9, 1052–1057.

236 Y. Lu, J. Zhao, R. Zhang, Y. Liu, D. Liu, E. M. Goldys, X. Yang, P. Xi, A. Sunna, J. Lu, Y. Shi, R. C. Leif, Y. Huo, J. Shen, J. a. Piper, J. P. Robinson and D. Jin, Nat. Photonics, 2013, 8, 32–36.

237 J. M. Meruga, A. Baride, W. Cross, J. J. Kellar and P. S. May, J. Mater. Chem. C, 2014, 2, 2221–2227.

238 A. L. Linsebigler, G. Lu and J. T. J. Yates, Chem. Rev., 1995, 95, 735–758.

239 K. Nakata and A. Fujishima, J. Photochem. Photobiol., C, 2012, 13, 169–189.

240 W. Qin, D. Zhang, D. Zhao, L. Wang and K. Zheng, Chem. Commun., 2010, 46, 2304–2306.

241 S. Obrego′n and G. Colo′n, Chem. Commun., 2012, 48, 7865–7867.

242 W. Wang, W. Huang, Y. Ni, C. Lu and Z. Xu, ACS Appl. Mater. Interfaces, 2014, 6, 340–348.

243 Y. Jia, Z. Zhou, Y. Wei, Z. Wu, J. Chen, Y. Zhang and Y. Liu, J. Appl. Phys., 2013, 114, 213903.

244 Y. Jia, Z. Zhou, Y. Wei, Z. Wu, H. Wang, J. Chen, Y. Zhang and Y. Liu, Smart Mater. Struct., 2013, 22, 125014.

245 Y. Zhang, G. Gao, H. L. W. Chan, J. Dai, Y. Wang and J. Hao, Adv. Mater., 2012, 24, 1729–1735.

246 Y. Y. Hui, X. Liu, W. Jie, N. Y. Chan, J. Hao, Y.-T. Hsu, L.-J. Li, W. Guo and S. P. Lau, ACS Nano, 2013, 7, 7126–7131.

247 G. Bai, Y. Zhang and J. Hao, Sci. Rep., 2014, 4, 5724–5729.